

Quantum repeaters and teleportation via entangled phase-modulated multimode coherent states

R. Goncharov^{1,2,3,*}, Alexei D. Kiselev^{1,2,4,†}, E.S. Moiseev,⁵ E. Samsonov,^{1,2,3} S.A. Moiseev,⁵
F. Kiselev,^{1,2,3} and V. Egorov^{1,2,3}


¹Quantum Information Laboratory, ITMO University, Kadetskaya Line, 3, Saint Petersburg 199034, Russia

²Leading Research Center “National Center for Quantum Internet”, ITMO University, Birzhevaya Line, 16, Saint Petersburg 199034, Russia

³SMARTS-Quanttelecom LLC, 6th Vasilyevskogo Ostrova Line, 59, Saint Petersburg 199178, Russia

⁴Laboratory of Quantum Processes and Measurements, ITMO University, Kadetskaya Line 3b, Saint Petersburg 199034, Russia

⁵Kazan Quantum Center, Kazan National Research Technical University, 18a Chetaeva Str., Kazan 420111, Russia

 (Received 20 March 2023; revised 27 July 2023; accepted 22 September 2023; published 11 October 2023)

We present a scheme of quantum repeater that uses entangled multimode coherent states that are obtained by electro-optic modulation of symmetric and antisymmetric Schrödinger cat states. Part of the generated entangled frequency modes is sent to a symmetric beam splitter at the central node, while the remaining modes are stored locally in quantum memories. The entangled coherent states between remote quantum memories are conditionally prepared by photon-counting measurements at the output channels of the beam splitter. We study how the effects of decoherence in the quantum channel affect statistics of photocounts and, for the heralding outcomes determined by the parity of photocounts, evaluate the probability of success and the fidelity of the prepared entanglement depending on the symmetry of input cat states. It is demonstrated that the generated entanglement can be employed for teleportation of the phase information from the modulated states that are utilized in quantum key distributions with subcarrier wave encoding.

DOI: [10.1103/PhysRevApplied.20.044030](https://doi.org/10.1103/PhysRevApplied.20.044030)

I. INTRODUCTION

Transferring a quantum state between remote parties is the primary purpose of quantum communication [1,2]. It lies at the heart of a variety of applications that include secure transfer of classical messages using quantum key distribution (QKD) [3,4], quantum metrology [5–7], and distributed computations [8,9].

One of the key problems of quantum communication is the generation of high-fidelity quantum states entangled between distant sites [1]. In the majority of approaches to this problem, photons represent information carriers that can function as flying qubits and the fundamental difficulty is that the photons are subject to losses (optical absorption) and other noise-induced perturbations present in photonic channels such as optical fibers and a turbulent atmosphere. This noise has a detrimental effect on the quality of entanglement generated between two remote parties leading to exponential decay of the entanglement degree with the

channel length. Owing to the exponential losses, for the photons propagating in optical fibers, the achievable distances are limited to about 200 km and the transmission of entanglement over global distances (thousands of kilometers) becomes a challenging task. The concept of quantum repeaters (QRs) was put forward in Ref. [10] as the method to overcome this limitation.

The mode of operation of QRs assumes that the transmission channel is divided into several segments (elementary links). The first step is to prepare entanglement between the two nodes (at the ends) of each link. Then, at the next step, entanglement swapping between neighboring links is used to transfer entanglement over significant distances to the target points of a quantum network.

There is a number of reviews focusing on different aspects of QRs [11–14]. For instance, the review in Ref. [11] focuses on the so-called Duan-Lukin-Cirac-Zoller protocol developed in Ref. [15] and its improvements. In this protocol, linear optics is combined with photon counting to perform needed operations and atomic ensembles are used as quantum memories (see Ref. [16] for a review). The primitives and fundamental components

*rkgoncharov@itmo.ru

†alexei.d.kiselev@gmail.com

needed for QRs along with the classification of QR protocols into three relevant generations are reviewed in Ref. [12]. Advantages and challenges of each generation of QRs determined by the methods utilized to suppress loss and operation errors are analyzed in Ref. [13]. A more recent review in Ref. [14] additionally discusses newly emerging classes of repeaters such as memoryless, error-corrected, and all-photon repeaters [17–19] and puts particular emphasis on the increasingly important role of QRs for the development of long-distance quantum networks (quantum internet) [20–22]. For such entanglement-assisted networks, the primary challenge is to go beyond the limit of point-to-point quantum communication, achieving high-rate secure communication without using trusted relay nodes.

Among a variety of photonic quantum states used in QR protocols, the coherent states have attracted considerable attention [23–25] as the states that are relatively easy to produce and control. The QR protocol analyzed in Ref. [23] uses hybrid entanglement where the coherent states are entangled with atomic (spin) qubits. On the other hand, the entanglement generation and swapping protocols studied in Refs. [24,25] are based on the entangled coherent states.

These states were originally introduced in Ref. [26] (see Ref. [27] for a review) and there is a number of quantum information processing tasks that can be performed using the entangled coherent states [28–32]. Multimode coherent states also provide a potentially promising source of multipartite entanglement [33,34] required by the quantum networks. In this paper the approach to QRs based on such states will be our primary concern.

More specifically, we present and theoretically study the scheme of a quantum repeater that uses multimode coherent states generated by the electro-optic modulation of Schrödinger cat states. This is the method that produces phase-coded multimode signals to perform the subcarrier wave (SCW) encoding that is proved to be useful in point-to-point [35–38], plug-and-play [39], continuous-variable (CV) QKD [40–42], and twin-field QKD [43]. The scope of this method is not limited to the above protocols and, owing to its robustness to environmental distortion of fiber line, interferometer-free scheme and multiplexing capacity, the SCW encoding is one of the promising approaches for quantum communication.

For such an electro-optic phase modulation-based method, we examine both the heralded entanglement generation in elementary links and the entanglement swapping procedures utilized for the creation and distribution of entanglement between broadband quantum memories (QMs) (reports on recent experimental developments in the rapidly developing field of QMs can be found in, e.g., Refs. [44–55]). As compared with QR schemes based on controlled beam splitters (see, e.g., [24]), the electro-optic phase modulator provides a more flexible tool. In practical

implementation, using such a tool opens up new possibilities such as the ability to control entanglement swapping by choosing different sidebands and quick adjustment of the mutual phase between Alice and Bob. An important feature of our QR model is that it can be associated with a real-life experimental detection scheme and its applicability goes beyond the scope of QR protocols. In order to demonstrate the latter, we additionally discuss the task of teleportation of the coherent state phase.

The paper is organized as follows. In Sec. II we present our modulator-based scheme of the elementary link and analytical model for the heralded entanglement generation procedure employed to produce coherent cat states entangled between remote nodes of the link. In Sec. III we analyze the performance of the proposed scheme and quality of the generated entanglement by evaluating the fidelity and probabilities of photocounts for heralding events. In this analysis we consider nonideal photodetectors and take into account effects of decoherence using the decoherence model that is typical for CV quantum channels with energy transfer to environmental modes. In Sec. IV we discuss the entanglement swapping technique used to create long-distance entanglement and its performance. In Sec. V we present a teleportation scheme that employs created entangled coherent states to transfer phase information encoded into SCW states between remote parties. Finally, we discuss and summarize our results in Sec. VI.

II. ELEMENTARY LINK

Figure 1 presents the optical scheme of an elementary link that creates entanglement between two remote nodes (Alice and Bob) using the phase modulation method. In this method, Alice and Bob utilize electro-optic phase modulators to produce local multimode entangled states by modulating superpositions of one-mode coherent states known as the Schrödinger cat states. An important advantage of using fast phase modulators is that Alice and Bob can actively control the output states by changing the modulation index and phase.

Referring to Fig. 1, after generation of the local modulated states, one of the frequency modes is sent to the central relay via spectral filtering while keeping other modes stored in quantum memories. In this section we perform our analysis assuming that the input (nonmodulated) state of the (central) carrier wave mode for Alice's and Bob's modulators, $|\mathcal{S}_A\rangle$ and $|\mathcal{S}_B\rangle$, are generally two different one-mode Schrödinger cat states of the form

$$|\mathcal{S}_A\rangle = |\Psi_{\nu'}(\alpha)\rangle, \quad |\mathcal{S}_B\rangle = |\Psi_{\nu}(\beta)\rangle, \quad \nu, \nu' \in \{+, -\}, \quad (1)$$

where $|\Psi_+(\alpha)\rangle$ and $|\Psi_-(\alpha)\rangle$ are the symmetric (even) and antisymmetric (odd) Schrödinger cats, respectively. These states were originally introduced in Ref. [56] as even and

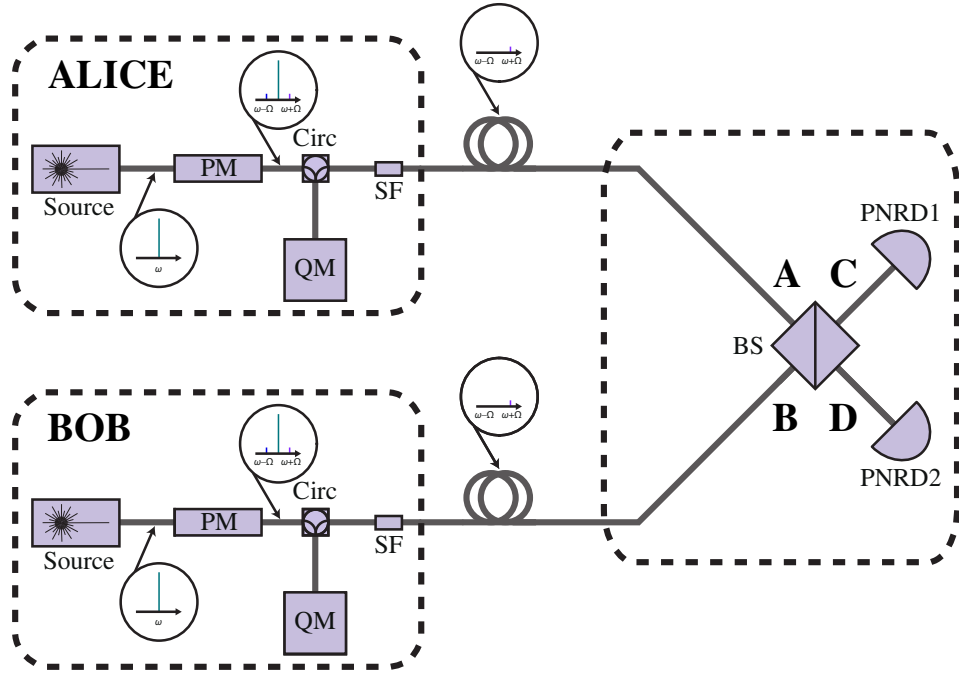


FIG. 1. Optical schematic of the subcarrier wave quantum repeater elementary link. Here source is a source of Schrödinger cat states, PM is the electro-optic modulator, Circ is the circulator, SF is the spectral filter, QM is the quantum memory, BS is the beam splitter, and PNRD is the photon-number-resolving detector. Diagrams in the circles show the absolute value of the signal spectrum taking into account only the first-order sidebands.

odd coherent states given by

$$|\Psi_{\pm}(\alpha)\rangle = \frac{1}{\sqrt{M_{\pm}(\alpha)}} |\alpha^{(\pm)}\rangle, \quad |\alpha^{(\pm)}\rangle \equiv |\alpha\rangle \pm |-\alpha\rangle, \quad (2)$$

where

$$M_{\pm}(\alpha) = \langle \alpha^{(\pm)} | \alpha^{(\pm)} \rangle = 2(1 \pm \exp(-2|\alpha|^2)). \quad (3)$$

There is a variety of experimental techniques used to generate optical Schrödinger cats [57–67]. It includes the method based on photon subtraction from the squeezed vacuum state [57–61], the protocol that uses homodyne detection and photon-number states [62], reservoir engineering [63–65], and the methods that involve making quadrature measurements of one of the modes of a biphoton NOON state [66] and reflecting coherent state photons from a microwave cavity containing a superconducting qubit [67].

According to the model of electro-optic modulator [68], for the input states $|\pm\alpha\rangle_A$ and $|\pm\beta\rangle_B$, the modulated states also known as the SCW states can be described as the multimode coherent states given by

$$|\pm\alpha\rangle_A \rightarrow |\pm\alpha\rangle_A = \otimes_{\mu=-S}^S |\pm\alpha_{\mu}\rangle_A, \quad (4)$$

$$|\pm\beta\rangle_B \rightarrow |\pm\beta\rangle_B = \otimes_{\mu=-S}^S |\pm\beta_{\mu}\rangle_B, \quad (4)$$

$$\alpha_{\mu} = U_{\mu 0}^{(A)*} \alpha, \quad \beta_{\mu} = U_{\mu 0}^{(B)*} \beta, \quad (5)$$

where $U_{\mu 0}^{(A,B)}$ are the elements of the evolution matrix. In the large S limit, these elements can be approximated as [68]

$$U_{\mu 0}^{(A,B)} \approx e^{-i\mu\phi_{A,B}} J_{\mu}(m_{A,B}), \quad (6)$$

where $\phi_{A,B}$ and $m_{A,B}$ are the phases and the modulation indices, respectively.

From Eq. (4) it can be readily seen that the electro-optic modulator acts like a multiport beam splitter that transforms the one-mode cat states (1) into the multimode Schrödinger cat states of the form

$$|S_A\rangle \rightarrow |\Psi_A\rangle = |\Psi_{\nu'}^{(A)}(\alpha)\rangle, \quad |S_B\rangle \rightarrow |\Psi_B\rangle = |\Psi_{\nu}^{(B)}(\beta)\rangle, \quad (7)$$

where

$$|\Psi_{\pm}^{(A)}(\alpha)\rangle = \frac{1}{\sqrt{M_{\pm}(\alpha)}} |\alpha^{(\pm)}\rangle_A, \quad (8)$$

$$|\Psi_{\pm}^{(B)}(\beta)\rangle = \frac{1}{\sqrt{M_{\pm}(\beta)}} \{|\beta\rangle_B \pm |-\beta\rangle_B\}, \quad (8)$$

$$|\alpha^{(\pm)}\rangle_A = |\alpha\rangle_A \pm |-\alpha\rangle_A, \quad (9)$$

$$M_{\pm}(\alpha) = 2(1 \pm \exp(-2|\alpha|^2)), \quad |\alpha|^2 = \sum_{\mu=-S}^S |\alpha_{\mu}|^2. \quad (10)$$

Thus, the modulated state shared by Alice and Bob, $|\Psi_{AB}\rangle$, is the tensor product of two multimode Schrödinger cat states after Alice's and Bob's modulators: $|\Psi\rangle_{AB} = |\Psi_{v'}^{(A)}(\alpha)\rangle \otimes |\Psi_v^{(B)}(\beta)\rangle$. This state can be written in the form

$$\begin{aligned} |\Psi\rangle_{AB} &= \frac{1}{N_{AB}} \left\{ |\alpha, \beta\rangle_{AB} + v'v|-\alpha, -\beta\rangle_{AB} + v|\alpha, -\beta\rangle_{AB} \right. \\ &\quad \left. + v'|-\alpha, \beta\rangle_{AB} \right\} \\ &= \sqrt{\frac{M_{v'v}(\alpha, \beta)}{M_{v'}(\alpha)M_v(\beta)}} \left\{ |\Psi_{v'v}^{(AB)}(\alpha, \beta)\rangle \right. \\ &\quad \left. + v|\Psi_{v'v}^{(AB)}(\alpha, -\beta)\rangle \right\}, \end{aligned} \quad (11)$$

$$M_{\pm}(\alpha, \beta) = 2 \left\{ 1 \pm \exp[-2(|\alpha|^2 + |\beta|^2)] \right\}, \quad (12)$$

where $N_{AB} = \sqrt{M_{v'}(\alpha)M_v(\beta)}$ and $|\alpha, \beta\rangle_{AB}$ represents $|\alpha\rangle_A \otimes |\beta\rangle_B$ rearranged into the tensor product of modes.

From now on we restrict our analysis to the important special case where $\alpha = \beta$ and, following the general approach [11,24] to the preparation of entangled states shared by Alice and Bob, we assume that the modes α that enter the modulated states, $|\Psi_v(\alpha)\rangle \equiv |\Psi_v(\alpha_{\text{qm}}, \alpha_{\text{bs}})\rangle$, are divided into two groups: the modes α_{qm} stored in the quantum memory and the modes α_{bs} put to interfere onto a symmetric 50 : 50 beam splitter with the output channels C and D . The above modes brought into interference onto the beam splitter appear to be transformed as

$$\begin{aligned} \hat{T}_{\alpha_{\text{bs}}\alpha_{\text{bs}} \rightarrow CD} |\pm\alpha_{\text{bs}}\rangle_A \otimes |\pm\alpha_{\text{bs}}\rangle_B &= |\pm\gamma_{\text{bs}}\rangle_C \otimes |\mathbf{0}\rangle_D, \\ \hat{T}_{\alpha_{\text{bs}}\alpha_{\text{bs}} \rightarrow CD} |\pm\alpha_{\text{bs}}\rangle_A \otimes |\mp\alpha_{\text{bs}}\rangle_B &= |\mathbf{0}\rangle_C \otimes |\pm\gamma_{\text{bs}}\rangle_D, \end{aligned} \quad (13)$$

where $\gamma_{\text{bs}} = \sqrt{2}\alpha_{\text{bs}}$.

We can now apply transformation (13) to the state shared by Alice and Bob (see Eq. (11)). The result reads

$$\begin{aligned} \hat{T}_{\alpha_{\text{bs}}\alpha_{\text{bs}} \rightarrow CD} |\Psi_{v'}^{(A)}(\alpha_{\text{qm}}, \alpha_{\text{bs}})\rangle \otimes |\Psi_v^{(B)}(\alpha_{\text{qm}}, \alpha_{\text{bs}})\rangle &= \frac{1}{2\sqrt{M_{v'}(\alpha_{\text{qm}}, \alpha_{\text{bs}})M_v(\alpha_{\text{qm}}, \alpha_{\text{bs}})}} \\ &\times \sum_{\mu=\pm} \sqrt{M_{\mu'}(\gamma_{\text{bs}})M_{\mu}(\alpha_{\text{qm}}, \alpha_{\text{qm}})} \left\{ |\Psi_{\mu'}^{(C)}(\gamma_{\text{bs}})\rangle \otimes \text{ket}\mathbf{0}_D \otimes |\Psi_{\mu}^{(AB)}(\alpha_{\text{qm}}, \alpha_{\text{qm}})\rangle \right. \\ &\quad \left. + v|\mathbf{0}\rangle_C \otimes |\Psi_{\mu'}^{(D)}(\gamma_{\text{bs}})\rangle \otimes |\Psi_{\mu}^{(AB)}(\alpha_{\text{qm}}, -\alpha_{\text{qm}})\rangle \right\}, \quad \mu' = v v' \mu, \end{aligned} \quad (14)$$

where $\gamma_{\text{bs}} \equiv \sqrt{2}\alpha_{\text{bs}}$.

If, for instance, we now perform a measurement on the output mode C to distinguish the states $|\Psi_{v'v}^{(C)}(\gamma_{\text{bs}})\rangle$ and $|\Psi_{-v'v}^{(C)}(\gamma_{\text{bs}})\rangle$, the multimode state will collapse onto either $|\Psi_{+}^{(AB)}(\alpha_{\text{qm}}, \alpha_{\text{qm}})\rangle$ or $|\Psi_{-}^{(AB)}(\alpha_{\text{qm}}, \alpha_{\text{qm}})\rangle$, respectively. Thus, preparation of the entangled coherent cat states is heralded by the parity of clicks of a photon-number-resolving detector placed at the output channel C .

Now we introduce the modified symmetric cat state

$$|\tilde{\Psi}_{+}(\alpha)\rangle = \frac{1}{\sqrt{\tilde{M}_{+}(\alpha)}} \left[|\tilde{\alpha}\rangle + |-\tilde{\alpha}\rangle \right], \quad (15)$$

$$|\pm\tilde{\alpha}\rangle \equiv |\pm\alpha\rangle - e^{-|\alpha|^2/2} |\mathbf{0}\rangle,$$

where $\tilde{M}_{+}(\alpha) = M_{+}(\alpha) - 4 \exp(-|\alpha|^2)$, defined in terms of the coherent states renormalized by subtracting the vacuum contribution. Then we have a set of three orthonormal states: $|\Psi_{-}(\sqrt{2}\alpha_{\text{bs}})\rangle \equiv |\Phi_{-}(\gamma_{\text{bs}})\rangle$, $|\tilde{\Psi}_{+}(\sqrt{2}\alpha_{\text{bs}})\rangle \equiv |\Phi_{+}(\gamma_{\text{bs}})\rangle$, and $|\mathbf{0}\rangle$ that can be conveniently used to render

state (14) into the form

$$\begin{aligned} \hat{T}_{\alpha_{\text{bs}}\alpha_{\text{bs}} \rightarrow CD} |\Psi_{v'}^{(A)}(\alpha_{\text{qm}}, \alpha_{\text{bs}})\rangle \otimes |\Psi_v^{(B)}(\alpha_{\text{qm}}, \alpha_{\text{bs}})\rangle &= \sqrt{P_0^{(v'v)}} |\mathbf{0}, \mathbf{0}\rangle_{CD} \otimes |\Psi_{v'}^{(A)}(\alpha_{\text{qm}})\rangle \otimes |\Psi_v^{(B)}(\alpha_{\text{qm}})\rangle \\ &\quad + \sum_{\mu=\pm} \sqrt{P_{\mu}^{(v'v)}} \{ |\Phi_{\mu'}^{(C)}(\gamma_{\text{bs}})\rangle \otimes |\mathbf{0}\rangle_D \\ &\quad \otimes |\Psi_{\mu}^{(AB)}(\alpha_{\text{qm}}, \alpha_{\text{qm}})\rangle + v|\mathbf{0}\rangle_C \otimes |\Phi_{\mu'}^{(D)}(\gamma_{\text{bs}})\rangle \\ &\quad \otimes |\Psi_{\mu}^{(AB)}(\alpha_{\text{qm}}, -\alpha_{\text{qm}})\rangle \}, \end{aligned} \quad (16)$$

where $P_{\mu}^{(v'v)}$ is the probability for the states $|\Phi_{\mu'}(\gamma_{\text{bs}})\rangle_C \otimes |\mathbf{0}\rangle_D$ and $|\mathbf{0}\rangle_C \otimes |\Phi_{\mu'}(\gamma_{\text{bs}})\rangle_D$ to be detected at the output ports of the beam splitter, whereas $P_0^{(v'v)}$ is the probability to detect the vacuum state $|\mathbf{0}\rangle_C \otimes |\mathbf{0}\rangle_D$. So, we have

$$2P_{+}^{(v'v)} + 2P_{-}^{(v'v)} + P_0^{(v'v)} = 1 \quad (17)$$

and the expressions for $P_\mu^{(v'v)}$ are given by

$$\begin{aligned} P_\mu^{(v'v)} &= \text{Prob}(\mu|v'v) \\ &= \frac{1}{4} \frac{\tilde{M}_{\mu'}(\boldsymbol{\gamma}_{\text{bs}})M_\mu(\boldsymbol{\alpha}_{\text{qm}}, \boldsymbol{\alpha}_{\text{qm}})}{M_{v'}(\boldsymbol{\alpha}_{\text{qm}}, \boldsymbol{\alpha}_{\text{bs}})M_v(\boldsymbol{\alpha}_{\text{qm}}, \boldsymbol{\alpha}_{\text{bs}})}, \quad \mu \in \{+, -\}, \end{aligned} \quad (18a)$$

$$\begin{aligned} P_0^{(v'v)} &= \text{Prob}(0|v'v) \\ &= \frac{M_{v'}(\boldsymbol{\alpha}_{\text{qm}})M_v(\boldsymbol{\alpha}_{\text{qm}})}{M_{v'}(\boldsymbol{\alpha}_{\text{qm}}, \boldsymbol{\alpha}_{\text{bs}})M_v(\boldsymbol{\alpha}_{\text{qm}}, \boldsymbol{\alpha}_{\text{bs}})} \exp(-|\boldsymbol{\gamma}_{\text{bs}}|^2). \end{aligned} \quad (18b)$$

In the case where the modulated cat states are identical with $v = v'$, Eqs. (18) can be simplified giving the probabilities $P_\mu^{(vv)} \equiv P_\mu^{(v)}$ in the form

$$P_\pm^{(+)} = \tanh^2 |\alpha|^2 P_\pm^{(-)}, \quad (19a)$$

$$|\alpha|^2 = |\boldsymbol{\alpha}|^2 = |\boldsymbol{\alpha}_{\text{qm}}|^2 + |\boldsymbol{\alpha}_{\text{bs}}|^2, \quad |\boldsymbol{\alpha}_{\text{bs}}|^2 = r_{\text{bs}} |\alpha|^2, \quad (19b)$$

$$P_-^{(-)}(r_{\text{bs}}, |\alpha|^2) = \frac{\sinh(2(1-r_{\text{bs}})|\alpha|^2) \sinh(2r_{\text{bs}}|\alpha|^2)}{4 \sinh^2(|\alpha|^2)}, \quad (19c)$$

$$P_+^{(-)}(r_{\text{bs}}, |\alpha|^2) = \frac{\cosh(2(1-r_{\text{bs}})|\alpha|^2) \sinh^2(r_{\text{bs}}|\alpha|^2)}{2 \sinh^2(|\alpha|^2)}, \quad (19d)$$

$$\begin{aligned} P_0^{(-)}(r_{\text{bs}}, |\alpha|^2) &= \frac{\sinh^2((1-r_{\text{bs}})|\alpha|^2)}{\sinh^2(|\alpha|^2)}, \\ P_0^{(+)}(r_{\text{bs}}, |\alpha|^2) &= \frac{\cosh^2((1-r_{\text{bs}})|\alpha|^2)}{\cosh^2(|\alpha|^2)}, \end{aligned} \quad (19e)$$

where the parameter r_{bs} is the ratio of the average number of photons for the modes sent to the beam splitter, $|\boldsymbol{\alpha}_{\text{bs}}|^2/|\boldsymbol{\alpha}|^2$, and the input mean photon number, $|\alpha|^2 = |\boldsymbol{\alpha}|^2$. In the opposite case with modulated cat states that differ in symmetry, the probabilities $P_\mu^{(+ -)} = P_\mu^{(- +)} \equiv P_\mu^{(c)}$ are given by

$$P_-^{(c)}(r_{\text{bs}}, |\alpha|^2) = \frac{\sinh(2(1-r_{\text{bs}})|\alpha|^2) \sinh^2(r_{\text{bs}}|\alpha|^2)}{\sinh(2|\alpha|^2)}, \quad (20a)$$

$$P_+^{(c)}(r_{\text{bs}}, |\alpha|^2) = \frac{\cosh(2(1-r_{\text{bs}})|\alpha|^2) \sinh(2r_{\text{bs}}|\alpha|^2)}{2 \sinh(2|\alpha|^2)}, \quad (20b)$$

$$P_0^{(c)}(r_{\text{bs}}, |\alpha|^2) = \frac{\sinh(2(1-r_{\text{bs}})|\alpha|^2)}{\sinh(2|\alpha|^2)}. \quad (20c)$$

From Eq. (19b), the probabilities for two antisymmetric cat states $P_\pm^{(-)}$ are higher than those describing the case of two symmetric cats, $P_\pm^{(+)}$. In particular, at small values of

$|\alpha|$, the latter is proportional to $|\alpha|^2$, whereas, for $P_\pm^{(-)}$, we have

$$P_-^{(-)} \approx r_{\text{bs}}(1-r_{\text{bs}}), \quad P_+^{(-)} \approx r_{\text{bs}}^2/2. \quad (21)$$

Note that the relations

$$P_-^{(c)} \approx r_{\text{bs}}(1-r_{\text{bs}})^2|\alpha|^4, \quad P_+^{(c)} \approx r_{\text{bs}}/2 \quad (22)$$

describe the behavior of $P_\pm^{(c)}$ in the region of small amplitudes $|\alpha|$.

Now we briefly discuss how the photon-number ratio r_{bs} affects $|\alpha|^2$ dependence of the probabilities. Figure 2 shows the surfaces representing the probabilities $P_\pm^{(-)}$ and $P_\pm^{(c)}$ plotted in the $r_{\text{bs}}-|\alpha|^2$ plane.

At $0 < r_{\text{bs}} < 1$, all the probabilities $P_\pm^{(+)}$, $P_\pm^{(-)}$, and $P_\pm^{(c)}$ approach the value 1/4 in the limit of large amplitudes with $|\alpha| \rightarrow \infty$. They also vanish provided the ratio r_{bs} is zero. Obviously, in this case, we cannot produce entangled states.

From Eqs. (19) and (20), at $r_{\text{bs}} = 1$, the probabilities $P_{-,0}^{(-)}$ and $P_{-,0}^{(c)}$ equal zero, whereas $P_+^{(-)} = P_+^{(c)} = 1/2$. Another case where the probabilities $P_-^{(-)}$ and $P_+^{(c)}$ [see Eqs. (19c) and (20b)] are independent of $|\alpha|$, $P_-^{(-)} = P_+^{(c)} = 1/4$ occurs at the ratio equal to one half, $r_{\text{bs}} = 1/2$.

III. PHOTODETECTION AND DECOHERENCE

In the previous section we found that generation of the entangled cat states is heralded by outcomes of measurements performed at the relay node in the orthonormal basis $\{|\Phi_+\rangle, |\Phi_-\rangle, |\mathbf{0}\rangle\}$. Such measurements would perfectly discriminate between the states at the output ports of the beam splitter producing the entangled states, $|\Psi_\pm^{(AB)}\rangle$, shared by the remote nodes of the link with the probabilities $P_\pm^{(vv')}$ conditioned on the symmetry of the input local states: $|\Psi_{v'}^{(A)}\rangle \otimes |\Psi_v^{(B)}\rangle$. In this section we extend our analysis to the cases where outcomes of the measurements are determined by the statistics of photocounts registered by the photodetector and decoherence-induced effects are taken into consideration.

A. Probability of photocounts

We begin with the decoherence effects for the states transmitted through the fiber channels from Alice and Bob to the beam splitter (central) node. The decoherence processes will affect the output states of the beam splitter, $|\Phi_\pm^{(S)}(\boldsymbol{\gamma}_{\text{bs}})\rangle = |\Phi_\pm^{(S)}(\boldsymbol{\gamma})\rangle$, where S stands for the output channel of the beam splitter (S is either C or D), that enter the right-hand side of Eq. (16). For simplicity, we restrict ourselves to the one-mode case with $|\Phi_\pm^{(S)}(\boldsymbol{\gamma}_{\text{bs}})\rangle = |\Phi_\pm^{(S)}(\boldsymbol{\gamma})\rangle$ and assume that the noisy channels are identical and represented by the well-known pure-loss bosonic

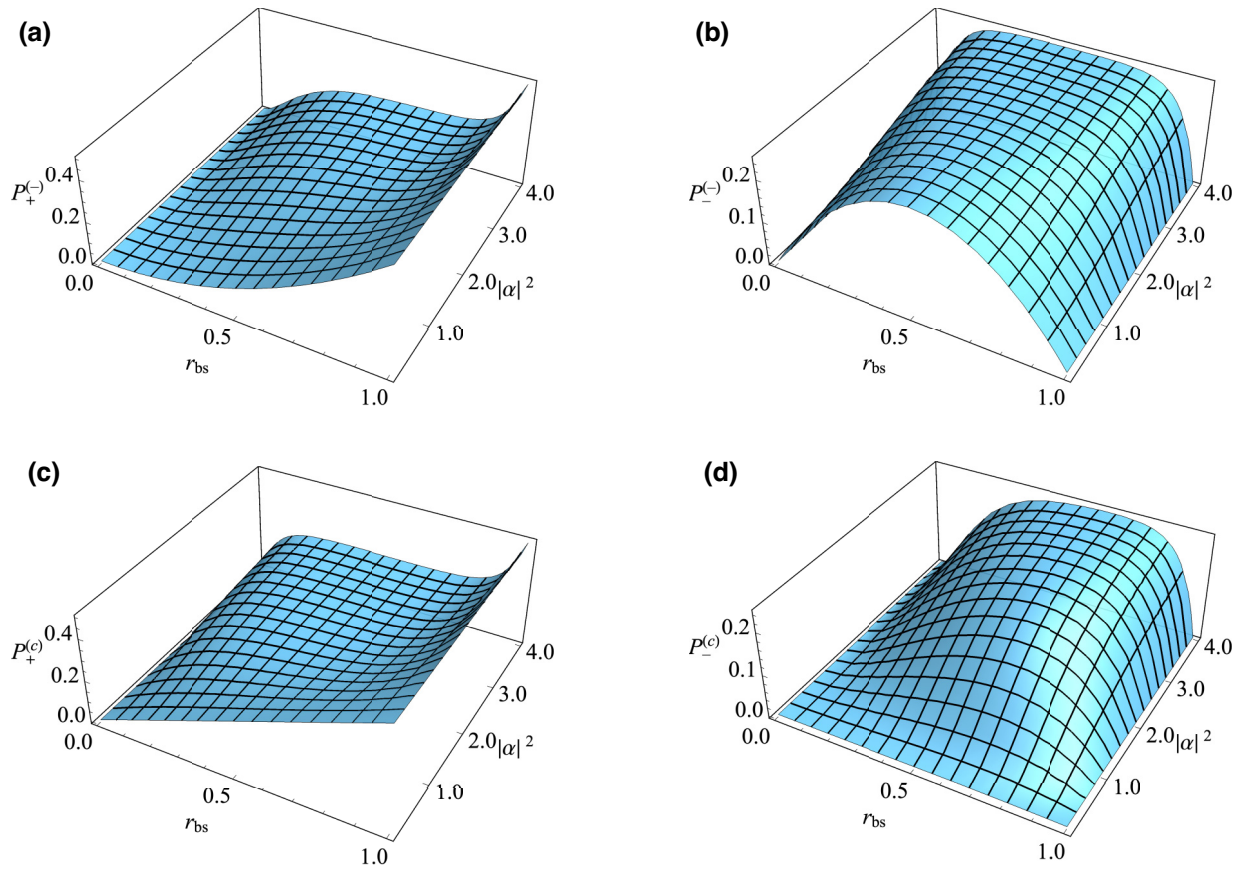


FIG. 2. Probabilities $P_{\pm}^{(-)}$ and $P_{\pm}^{(c)}$ associated with the cat states $|\Phi_{\pm}(\boldsymbol{\gamma}_{\text{bs}})\rangle$ at an output port of the beam splitter computed from Eqs. (19) and (20) as a function of $|\alpha|^2$ and $r_{\text{bs}} = |\alpha_{\text{bs}}|^2/|\alpha|^2$.

channel that can be described by introducing an additional environmental (ancillary) mode (see, e.g., Refs. [25,30]). An isometry representing the Stinespring dilation of the fiber channel where the signal mode is supplemented with an extra system E (the channel's environment) is given by the mapping

$$\begin{aligned} |\boldsymbol{\gamma}\rangle_S &\rightarrow |\boldsymbol{\gamma}_s\rangle_S \otimes |\boldsymbol{\gamma}_e\rangle_E = |\boldsymbol{\gamma}_s, \boldsymbol{\gamma}_e\rangle \equiv |\boldsymbol{\gamma}\rangle, \\ |\boldsymbol{\gamma}|^2 &= |\boldsymbol{\gamma}_s|^2 + |\boldsymbol{\gamma}_e|^2, \end{aligned} \quad (23)$$

where $|\boldsymbol{\gamma}_s|^2 = \eta|\boldsymbol{\gamma}|^2$ and $|\boldsymbol{\gamma}_e|^2 = (1 - \eta)|\boldsymbol{\gamma}|^2$; $\eta = \exp(-L/L_{\text{att}})$ is the fiber transmittance, L is the fiber length, and L_{att} is the attenuation length. Note that, the pure-loss channel provides a simplified model of light propagation in a fiber, where a number of polarization and dispersion dependent effects are not taken in account.

One of the methods to discriminate between the symmetric and antisymmetric cat states is to perform photon-counting measurements that may distinguish the parity of the photon number registered by a photodetector. For a photon-number-resolving photodetector, the probability to detect k photons in the signal mode conditioned on the event that the initial state $|\Psi_{\nu'}^{(A)}\rangle \otimes |\Psi_{\nu}^{(B)}\rangle$ is projected onto

the entangled state $|\Psi_{\mu}^{(AB)}\rangle$ is

$$\text{Prob}(k|\mu, \nu'\nu) = P(k|\mu'), \quad \mu' = \nu'\nu\mu, \quad (24)$$

which is expressed in terms of the probability of clicks $P(k|\mu)$ determined by the statistics of photocounts for the cat states $|\Phi_{\mu}(\boldsymbol{\gamma})\rangle$. According to the well-known Kelley-Kleiner formula [69,70], this probability reads

$$P(k|\mu) = \langle \Phi_{\mu}(\boldsymbol{\gamma}) | \hat{\Pi}_k | \Phi_{\mu}(\boldsymbol{\gamma}) \rangle, \quad P(k|0) = \delta_{k0}, \quad (25)$$

where $\hat{\Pi}_k$ is the positive operator-valued measure for a number-resolving detector given by

$$\hat{\Pi}_k =: \frac{(\xi \hat{n}_s)^k}{k!} e^{-\xi \hat{n}_s} \cdot, \quad \hat{n}_s = \hat{a}_s^{\dagger} \hat{a}_s, \quad (26)$$

where ξ is the efficiency of the detector. We can now apply the algebraic identity

$$\begin{aligned} \text{Tr}_E |\boldsymbol{\gamma}^{(\pm)}\rangle \langle \boldsymbol{\gamma}^{(\pm)}| &= \frac{1}{4} \{ M_{\pm}(\boldsymbol{\gamma}_e) |\boldsymbol{\gamma}_s^{(+)}\rangle \langle \boldsymbol{\gamma}_s^{(+)}| \\ &\quad + M_{\mp}(\boldsymbol{\gamma}_e) |\boldsymbol{\gamma}_s^{(-)}\rangle \langle \boldsymbol{\gamma}_s^{(-)}| \} \end{aligned} \quad (27)$$

to deduce the following expressions of probabilities (25):

$$P(k|+) = \frac{1}{4\tilde{M}_+(\boldsymbol{\gamma})} \{M_+(\gamma_e)C_+(k, \gamma_s) + M_-(\gamma_e)C_-(k, \gamma_s)\}, \quad k > 0, \quad (28)$$

$$P(k|-) = \frac{1}{4\tilde{M}_-(\boldsymbol{\gamma})} \{M_-(\gamma_e)C_+(k, \gamma_s) + M_+(\gamma_e)C_-(k, \gamma_s)\}, \quad P(k|0) = 0. \quad (29)$$

Here

$$C_\mu(k, \gamma_s) = \langle \gamma_s^{(\mu)} | \hat{\Pi}_k | \gamma_s^{(\mu)} \rangle = 2 \frac{(\xi |\gamma_s|^2)^k}{k!} e^{-|\gamma_s|^2} \left\{ e^{(1-\xi)|\gamma_s|^2} + (-1)^k \mu e^{-(1-\xi)|\gamma_s|^2} \right\}. \quad (30)$$

In what follows, we consider the heralding outcomes described by the two different parity of clicks, $p_c \in \{\text{even}, \text{odd}\}$, and thus, discriminate between the cases, where the number of registered photons is either odd or even. The sum of the corresponding probabilities

$$P(\text{even}|\pm, 0) = \sum_{n=1}^{\infty} P(2n|\pm, 0), \quad (31)$$

$$P(\text{odd}|\pm, 0) = \sum_{n=0}^{\infty} P(2n+1|\pm, 0),$$

and the no-click probability, $P(0|\mu)$, gives unity and we have the completeness identity

$$P(0|\pm, 0) + P(\text{even}|\pm, 0) + P(\text{odd}|\pm, 0) = 1. \quad (32)$$

By substituting Eqs. (28)–(30) into relations (31) we obtain the expressions for the probabilities of the detection outcomes determined by the parity of clicks

$$P(p_c|+) = \frac{1}{4\tilde{M}_+(\boldsymbol{\gamma})} \{M_+(\gamma_e)C_+(p_c, \gamma_s) + M_-(\gamma_e)C_-(p_c, \gamma_s)\}, \quad p_c \in \{\text{even}, \text{odd}\}, \quad (33a)$$

$$P(p_c|-) = \frac{1}{4\tilde{M}_-(\boldsymbol{\gamma})} \{M_-(\gamma_e)C_+(p_c, \gamma_s) + M_+(\gamma_e)C_-(p_c, \gamma_s)\}, \quad P(p_c|0) = 0, \quad (33b)$$

where

$$C_\pm(\text{even}, \gamma_s) = 2e^{-|\gamma_s|^2} (\cosh(\xi |\gamma_s|^2) - 1) \times \left\{ e^{(1-\xi)|\gamma_s|^2} \pm e^{-(1-\xi)|\gamma_s|^2} \right\}, \quad (34a)$$

$$C_\pm(\text{odd}, \gamma_s) = 2e^{-|\gamma_s|^2} \sinh(\xi |\gamma_s|^2) \times \left\{ e^{(1-\xi)|\gamma_s|^2} \mp e^{-(1-\xi)|\gamma_s|^2} \right\}. \quad (34b)$$

It can be checked that these relations meet the algebraic identity

$$\frac{P(\text{even}|-)P_-^{(\pm)}}{P(\text{even}+)P_+^{(\pm)}} = \frac{P(\text{odd}+)P_-^{(c)}}{P(\text{odd}|-)P_+^{(c)}}. \quad (35)$$

They can also be readily generalized to the case of a multi-mode signal, where $|\gamma_s\rangle \rightarrow |\boldsymbol{\gamma}_s\rangle \equiv |\gamma_1^{(s)}, \dots, \gamma_{N_s}^{(s)}\rangle$ and N_s is the number of signal modes registered by a broadband detector, by replacing $|\gamma_s|^2$ and $\xi |\gamma_s|^2$ with $|\boldsymbol{\gamma}_s|^2 = \sum_{i=1}^{N_s} |\gamma_i^{(s)}|^2$ and $\sum_{i=1}^{N_s} \xi_i |\gamma_i^{(s)}|^2$.

Referring to Fig. 3, it is seen that, for the limiting case of the ideal photodetector and the lossless channel with the efficiency and the transmittance both equal to

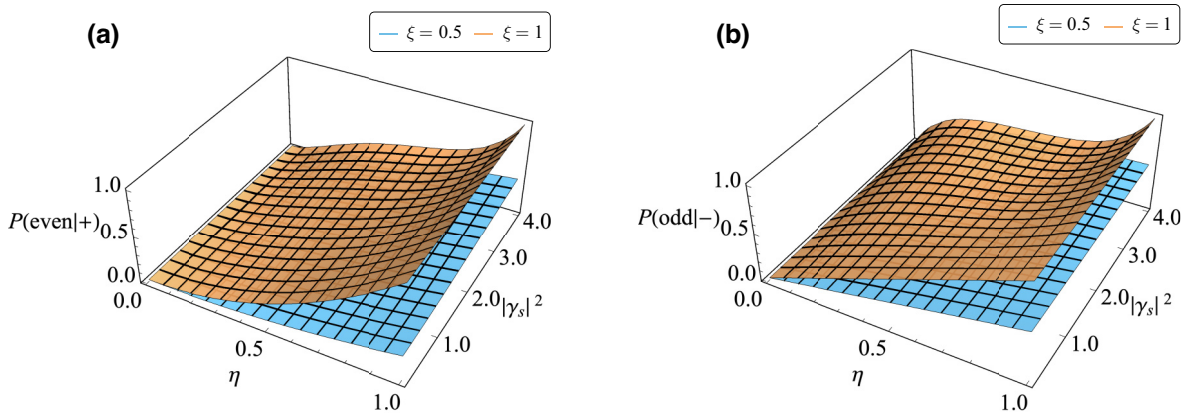


FIG. 3. Conditional probabilities (a) $P(\text{even}|+)$ and (b) $P(\text{odd}|-)$ plotted against the mean photon number $|\gamma_s|^2$ and the channel transmittance η at different values of the detection efficiency ξ .

unity, $\xi = \eta = 1$, the probability of an odd (even) number of clicks vanishes for the symmetric (antisymmetric) states, $P(\text{odd}|+) = 0$ ($P(\text{even}|-) = 0$), and thus, the cat states are perfectly distinguishable with $P(\text{even}|+) = 1$ ($P(\text{odd}|-) = 1$). It can also be noted that low detector efficiency ξ has a noticeable detrimental effect on the conditional probabilities.

B. Performance and entanglement

We can now evaluate the probability of success for the heralding outcomes labeled by the parity p_c . Similar to all other probabilities, this probability is conditioned on the symmetry of the initial states and can be written in the following general form:

$$P_s^{(v'v)}(p_c) = \sum_{\mu=\pm} \text{Prob}(p_c|\mu, v'v)\text{Prob}(\mu|v'v) = \sum_{\mu=\pm} P(p_c|\mu')P_\mu^{(v'v)}. \quad (36)$$

After substituting formulas given by Eqs. (19), (20), and (33) into Eq. (36) and performing cumbersome but

rather straightforward algebra, it can be shown that $P_\pm^{(v'v)}$ with the photon-number ratio r_{bs} replaced by the product $\zeta = \xi\eta r_{\text{bs}}$ give explicit expressions for the probabilities of success $P_s^{(v'v)}$ as

$$P_s^{(+)}(p_c) = \tanh^2(|\alpha|^2)P_s^{(-)}(p_c), \quad (37a)$$

$$P_s^{(-)}(\text{odd}) = P_-^{(-)}(\zeta, |\alpha|^2), \quad P_s^{(+)}(\text{odd}) = P_+^{(+)}(\zeta, |\alpha|^2), \quad (37b)$$

$$P_s^{(-)}(\text{even}) = P_+^{(-)}(\zeta, |\alpha|^2), \quad P_s^{(+)}(\text{even}) = P_-^{(+)}(\zeta, |\alpha|^2), \quad (37c)$$

where $P_\mp^{(-)}$ and $P_\mp^{(+)}$ are given by Eqs. (19c) and (19d) and Eqs. (20a) and (20b), respectively.

These relations imply that the results presented at the end of Sec. III are directly applicable to the success probabilities. As is shown in Fig. 4, in the limit of vanishing α , the largest probabilities of success $P_s^{(-)}(\text{odd})$ and $P_s^{(+)}(\text{odd})$ take the values $\zeta(1 - \zeta)$ and $\zeta/2$, respectively. As the amplitude $|\alpha|$ increases, the probabilities vary approaching the limiting value equal to 1/4.

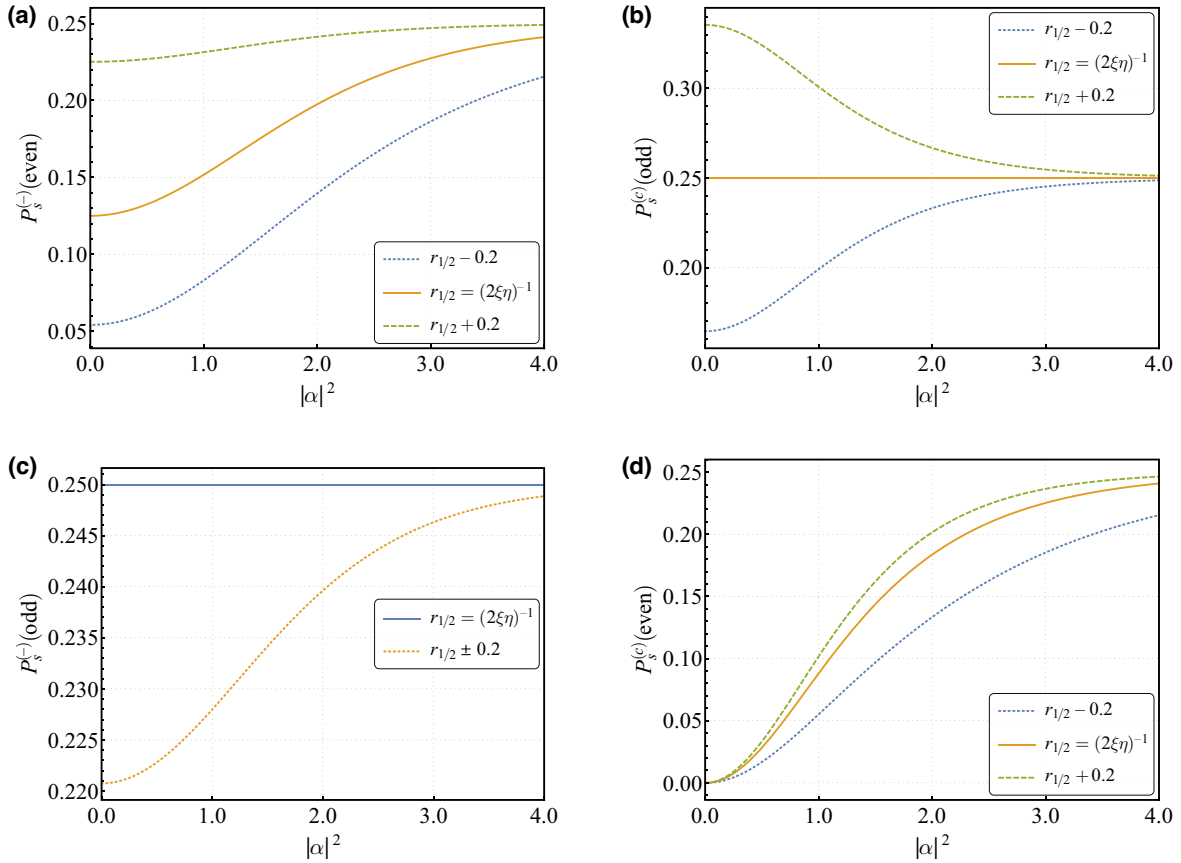


FIG. 4. The success probabilities $P_s^{(-)}(p_c)$ and $P_s^{(+)}(p_c)$ —the parity of photocounts is labeled by $p_c \in \{\text{even, odd}\}$ —of outcomes that herald the generation of predominantly (a),(b) symmetric and (c),(d) antisymmetric cat states with $F_+^{(v'v)} > 1/2$ and $F_-^{(v'v)} > 1/2$, respectively. The curves are computed at $r_{\text{bs}} \in \{r_{1/2}, r_{1/2} \pm 0.2\}$ with $\eta = 0.95$ and $\xi = 0.9$, where $r_{1/2} \equiv (2\xi\eta)^{-1}$ ($\zeta = 1/2$).

Given the heralding event p_c , the heralded state is represented by the density matrix

$$\hat{\rho}_{AB}^{(v'v)}(p_c) = \sum_{\mu=\pm} F_{\mu}^{(v'v)}(p_c) |\Psi_{\mu}^{(AB)}(\alpha_{\text{qm}}, \alpha_{\text{qm}})\rangle \times \langle \Psi_{\mu}^{(AB)}(\alpha_{\text{qm}}, \alpha_{\text{qm}})|, \quad (38)$$

where $F_{\mu}^{(v'v)} = \langle \Psi_{\mu}^{(AB)} | \hat{\rho}_{AB}^{(v'v)} | \Psi_{\mu}^{(AB)} \rangle$ are the fidelities that can be computed using the well-known Bayesian formula

$$\begin{aligned} F_{\mu}^{(v'v)}(p_c) &= \text{Prob}(\mu | p_c, v'v) \\ &= \frac{\text{Prob}(p_c | \mu, v'v) \text{Prob}(\mu | v'v)}{P_s^{(v'v)}(p_c)} \\ &= \frac{P(p_c | \mu') P_{\mu}^{(v'v)}}{P_s^{(v'v)}(p_c)} \end{aligned} \quad (39)$$

and meet the symmetry condition

$$F_{\mu}^{(\pm)}(\text{even/odd}) = F_{\mu}^{(c)}(\text{odd/even}) \quad (40)$$

that is a direct consequence of identity (35). Similar to Eqs. (37a)–(37c), after tedious algebra, we derive the following expressions for the fidelities:

$$\begin{aligned} F_{-}^{(\pm)}(\text{odd}) &= F_{-}^{(c)}(\text{even}) \\ &= \frac{\tanh(2(1 - r_{\text{bs}})|\alpha|^2)}{\tanh(2(1 - r_{\text{bs}})|\alpha|^2) + \tanh(2(r_{\text{bs}} - \zeta)|\alpha|^2)}, \end{aligned} \quad (41a)$$

$$\begin{aligned} F_{+}^{(\pm)}(\text{even}) &= F_{+}^{(c)}(\text{odd}) \\ &= \frac{1}{1 + \tanh(2(1 - r_{\text{bs}})|\alpha|^2) \tanh(2(r_{\text{bs}} - \zeta)|\alpha|^2)}. \end{aligned} \quad (41b)$$

Note that, owing to the completeness condition $F_{+}^{(v'v)}(p_c) + F_{-}^{(v'v)}(p_c) = 1$ and the symmetry relations in Eq. (40),

we need to specify only two fidelities. These fidelities $F_{-}^{(\pm)}$ (odd) and $F_{+}^{(\pm)}$ (even) are both above 1/2 and represent predominantly the antisymmetric and symmetric cat states, respectively. From $|\alpha|^2$ dependencies of $F_{-}^{(\pm)}$ (odd) and $F_{+}^{(\pm)}$ (even) depicted in Fig. 5, both the fidelities start from their zero-amplitude values

$$F_{+}^{(\pm)}(\text{even}, \alpha = 0) = 1, \quad F_{-}^{(\pm)}(\text{odd}, \alpha = 0) = \frac{1 - r_{\text{bs}}}{1 - \zeta}, \quad (42)$$

and decay approaching 1/2 with the amplitude $|\alpha|$.

At $r_{\text{bs}} = r_{1/2} \equiv (2\eta\xi)^{-1}$, we have $\zeta = 1/2$, so that $2P_s^{(c)}$ (odd) and $2P_s^{(-)}$ (odd) equal 1/2 (see Fig. 4) as the probabilities of the most probable outcomes heralding generation of the symmetric and antisymmetric cat states with the fidelities $F_{+}^{(\pm)}$ (even) and $F_{-}^{(\pm)}$ (odd), respectively. In this case, Eq. (42) gives unity and $1/(2 - \eta\xi)$ as the maximum values of $F_{+}^{(\pm)}$ (even) and $F_{-}^{(\pm)}$ (odd).

Interestingly, $F_{+}^{(\pm)}$ (even, $\alpha = 0$) does not depend on the parameters, whereas the maximum value of $2P_s^{(c)}$ (odd) is ζ provided the photon-number ratio r_{bs} is above $(2\eta\xi)^{-1}$. By contrast, when $r_{\text{bs}} \neq (2\eta\xi)^{-1}$, the probability $2P_s^{(-)}$ (odd) [it equals $(1 - (2\zeta - 1)^2)/2$ at $\alpha = 0$] cannot exceed one half and the fidelity $F_{-}^{(\pm)}$ (odd, $\alpha = 0$) grows as the ratio r_{bs} becomes smaller than $(2\eta\xi)^{-1}$.

IV. ENTANGLEMENT SWAPPING

In this section we discuss the entanglement swapping protocol that uses the heralded entanglement generation procedure studied in the previous section to create entanglement between remote points of two elementary links, $A_1 - B_1$ and $B_2 - A_2$, depicted in Fig. 6. In our subsequent analysis we consider the structure where the neighboring end nodes, B_1 and B_2 , of the adjacent links, $A_1 - B_1$ and

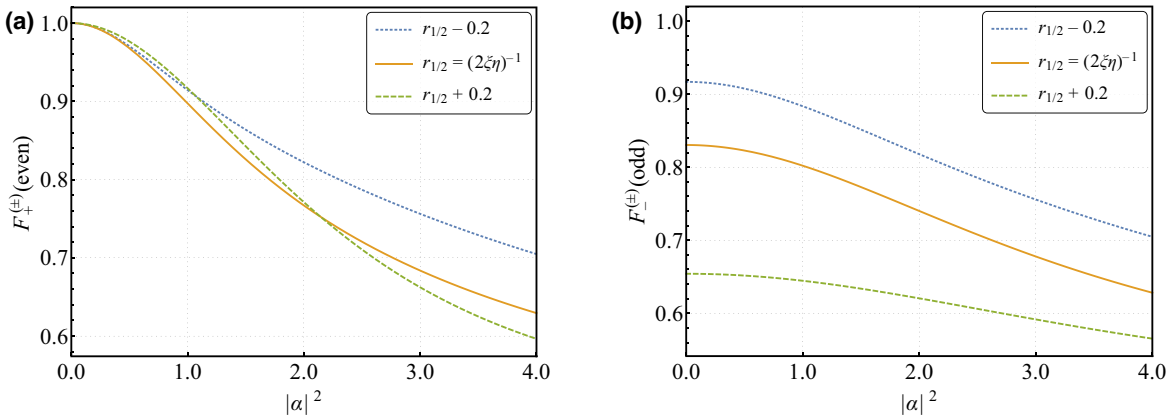


FIG. 5. Fidelities of heralded symmetric and antisymmetric cat states: (a) $F_{+}^{(\pm)}$ (even) and (b) $F_{-}^{(\pm)}$ (odd) as a function of $|\alpha|^2$ computed at different values of r_{bs} (the parameters are listed in the caption of Fig. 4).

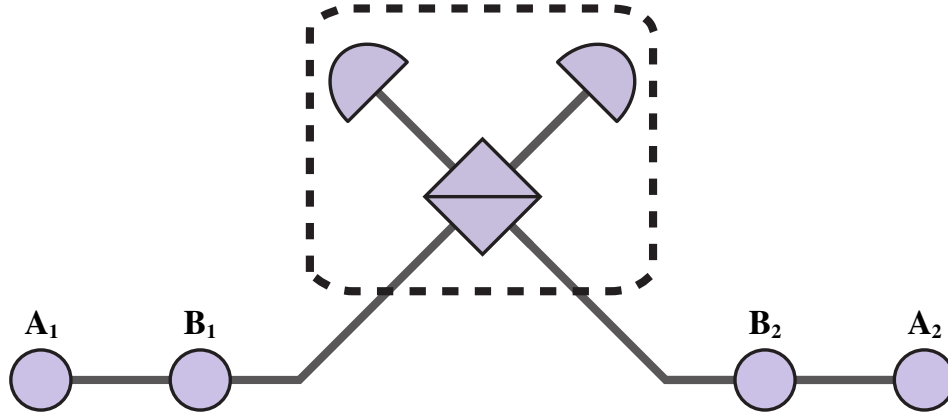


FIG. 6. Entanglement swapping scheme. Here $A_1 - B_1$ and $B_2 - A_2$ are adjacent elementary links.

$B_2 - A_2$, are located at the repeater station (the repeater node B_1B_2).

According to Eq. (38), the phase-modulated entangled states shared between the nodes of the links are described by the density matrices of the form

$$\hat{\rho}_{A_1B_1}^{(v'_1v_1)}(p_c) \equiv \hat{\rho}_1 = \sum_{\mu_1=\pm} F_{\mu_1}^{(1)} |\Psi_{\mu_1}^{(A_1B_1)}(\alpha_{\text{qm}}, \alpha_{\text{qm}})\rangle \times \langle \Psi_{\mu_1}^{(A_1B_1)}(\alpha_{\text{qm}}, \alpha_{\text{qm}}) |, \quad (43a)$$

$$\hat{\rho}_{A_2B_2}^{(v'_2v_2)}(p_c) \equiv \hat{\rho}_2 = \sum_{\mu_2=\pm} F_{\mu_2}^{(2)} |\Psi_{\mu_2}^{(A_2B_2)}(\alpha_{\text{qm}}, \alpha_{\text{qm}})\rangle \times \langle \Psi_{\mu_2}^{(A_2B_2)}(\alpha_{\text{qm}}, \alpha_{\text{qm}}) |, \quad (43b)$$

where $F_{\mu_i}^{(i)} \equiv F_{\mu_i}^{(v'_i v_i)}$, and $\hat{\rho}_1 \otimes \hat{\rho}_2$ is the initial state of the two-link system. So, the initial state is the statistical ensemble of the quantum states

$$|\Psi_{\mu_1\mu_2}^{(A_1B_1, A_2B_2)}\rangle \equiv |\Psi_{\mu_1}^{(A_1B_1)}(\alpha_{\text{qm}}, \alpha_{\text{qm}})\rangle \otimes |\Psi_{\mu_2}^{(A_2B_2)}(\alpha_{\text{qm}}, \alpha_{\text{qm}})\rangle \quad (44)$$

with the probabilities $F_{\mu_1}^{(1)} F_{\mu_2}^{(2)}$.

When the modes stored in the quantum memories of the sites B_1 and B_2 are released and sent to the beam splitter, the transformed state for each member of the ensemble is given by the general formula in Eq. (16). Similar to Sec. III A, we assume that the heralding events of the photocounting measurements are determined by the parity of photodetector clicks, so that we may closely follow the line of reasoning presented in Sec. III A and III B to deduce the heralded state for each state $|\Psi_{\mu_1\mu_2}^{(A_1B_1, A_2B_2)}\rangle$ in the modified form of Eq. (38) with $|\Psi_{\mu}^{(AB)}\rangle$ and $(v'\nu)$ replaced with $|\Psi_{\mu}^{(A_1A_2)}\rangle$ and $(\mu_1\mu_2)$, respectively.

As for elementary links, the fidelities, $\tilde{F}_{\mu}^{(\mu_1\mu_2)}(p_c)$, and the probabilities, $\tilde{P}_s^{(\mu_1\mu_2)}(p_c)$, at the repeater node can be evaluated using Eqs. (41) and (37), respectively.

Since, at this node, the modes are evenly partitioned with $\alpha_{\text{bs}} = \alpha_{\text{qm}}$ and $|\alpha_{\text{bs}}|^2 = |\alpha_{\text{qm}}|^2 = (1 - r_{\text{bs}})|\alpha|^2$, the parameters $\{r_{\text{bs}}, |\alpha|^2\}$ should be accordingly changed as follows: $\{r_{\text{bs}}, |\alpha|^2\} \rightarrow \{1/2, 2(1 - r_{\text{bs}})|\alpha|^2\}$.

For the measurements performed locally at the repeater node, the fiber transmission losses are negligible and the bulk part of losses can be attributed to inefficiency of the quantum memories. In order to take into account such losses, we, following a widely used phenomenological approach (see, e.g., Refs [21,71,72]), introduce the memory efficiency, η_m , as the parameter that replaces the transmission coefficient η . The latter implies that, similar to the effects of the fiber transmission losses and inefficiency of the photodetectors, decoherence effects in quantum memories are modeled using a pure-loss bosonic channel [see Eq. (23) in Sec. III A]. As a result, at the repeater node, the parameter ζ appears to be equal to the product $\eta_m \xi / 2$: $\zeta \rightarrow \zeta_m = \eta_m \xi / 2$.

The final result for the entanglement swapping transformation reads

$$\hat{\rho}_1 \otimes \hat{\rho}_2 \rightarrow \hat{\rho}_{12}(p_c) = \sum_{\mu=\pm} F_{\mu}^{(12)}(p_c) |\Psi_{\mu}^{(A_1A_2)}(\alpha_{\text{qm}}, \alpha_{\text{qm}})\rangle \times \langle \Psi_{\mu}^{(A_1A_2)}(\alpha_{\text{qm}}, \alpha_{\text{qm}}) |, \quad (45)$$

where $F_{\mu}^{(12)}(p_c)$ is the fidelity given by

$$\begin{aligned} F_{\mu}^{(12)}(p_c) &= \frac{1}{P_s^{(12)}(p_c)} \sum_{\mu_1, \mu_2=\pm} P(p_c | \mu_1 \mu_2 \mu) P_{\mu}^{(\mu_1 \mu_2)} F_{\mu_1}^{(1)} F_{\mu_2}^{(2)} \\ &= \frac{1}{P_s^{(12)}(p_c)} \sum_{\mu_1, \mu_2=\pm} \tilde{F}_{\mu}^{(\mu_1 \mu_2)}(p_c) \\ &\quad \times \tilde{P}_s^{(\mu_1 \mu_2)}(p_c) F_{\mu_1}^{(1)} F_{\mu_2}^{(2)}. \end{aligned} \quad (46)$$

It is rather straightforward to deduce the expression for the probabilities of success

$$\begin{aligned}
 P_s^{(12)}(p_c) &= \sum_{\mu, \mu_1, \mu_2 = \pm} \text{Prob}(p_c | \mu, \mu_1 \mu_2) \text{Prob}(\mu | \mu_1 \mu_2) \text{Prob}(\mu_1, \mu_2) \\
 &= \sum_{\mu, \mu_1, \mu_2 = \pm} P(p_c | \mu_1 \mu_2 \mu) P_\mu^{(\mu_1 \mu_2)} F_{\mu_1}^{(1)} F_{\mu_2}^{(2)} \\
 &= \sum_{\mu_1, \mu_2 = \pm} \tilde{P}_s^{(\mu_1 \mu_2)}(p_c) F_{\mu_1}^{(1)} F_{\mu_2}^{(2)}, \quad (47)
 \end{aligned}$$

where $\tilde{F}_\mu^{(\mu_1 \mu_2)}(p_c)$ ($\tilde{P}_s^{(\mu_1 \mu_2)}(p_c)$) is the above discussed fidelity (success probability) given by Eq. (41) [Eq. (37)] with the parameters $\{r_{\text{bs}}, \zeta, |\alpha|^2\}$ changed to $\{1/2, \eta_m \xi/2, 2(1 - r_{\text{bs}})|\alpha|^2\}$, which determine the performance of the protocol.

Our concluding remarks deal with analysis of the performance of a repeater with two links. To this end, we follow the method presented in Ref. [71] and start with the probabilities of success for the links

$$2P_s^{(v'_1 v_1)}(p_c)|_{A_1 B_1} \equiv p_1, \quad 2P_s^{(v'_2 v_2)}(p_c)|_{A_2 B_2} \equiv p_2 \quad (48)$$

that give the joint probability distribution for numbers of attempts as

$$P(n_1, n_2) = p_1 q_1^{n_1 - 1} p_2 q_2^{n_2 - 1}, \quad (49)$$

where $q_i = 1 - p_i$. An important point is that the entanglement swapping can be performed only after the entanglement is established in both links. Similar to Ref. [71], we take the assumption that the time required for each attempt is $T = L/c$, where L is the distance between the end nodes and the central node of an elementary link giving the length of the fiber channel and c is the speed of light. In our case, the length of the elementary link is $L_0 = 2L$, whereas the total repeater length is $L_{\text{tot}} = N_L L_0$, where N_L is the number of links.

From Eq. (48) it is not difficult to obtain the probability distribution for the magnitude of the difference in the number of attempts,

$$\text{Prob}(|n_1 - n_2| = k) = \frac{p_1 p_2 (q_1^k + q_2^k)}{2(1 - q_1 q_2)} (2 - \delta_{k0}) \quad (50)$$

and evaluate the expectation values

$$\begin{aligned}
 \langle n_w \rangle &\equiv \langle |n_1 - n_2| \rangle = \frac{p_2^2 q_1 + p_1^2 q_2}{p_1 p_2 (1 - q_1 q_2)}, \\
 \langle n_t \rangle &\equiv \langle n_1 + n_2 \rangle = \frac{p_1 + p_2}{p_1 p_2}, \quad (51)
 \end{aligned}$$

$$\begin{aligned}
 \langle n_{\text{max}} \rangle &\equiv \langle \max(n_1, n_2) \rangle = \frac{\langle n_t \rangle + \langle n_w \rangle}{2}, \\
 \langle n_{\text{min}} \rangle &\equiv \langle \min(n_1, n_2) \rangle = \frac{\langle n_t \rangle - \langle n_w \rangle}{2} \quad (52)
 \end{aligned}$$

that are related to the preparation and waiting times, T_{prep} and T_w , as [71]

$$T_{\text{prep}} = \langle n_{\text{max}} \rangle T, \quad T_w = \langle n_w \rangle T, \quad T = \frac{L}{c}. \quad (53)$$

For successful operation of the repeater, the waiting time is required to be shorter than the lifetime (alternatively, this time is called either the dephasing time or the coherence time) of the quantum memory: $T_w < T_m$. Under this condition, degradation of the generated entanglement has a negligible detrimental effect on the swapping protocol.

Figure 7 shows the $|\alpha|^2$ dependencies of the waiting times evaluated from Eqs. (51) and (53) assuming that the success probabilities for the links are both equal to either $P_s^{(-)}$ (odd) (the waiting time is $T_w^{(-)}$) or $P_s^{(c)}$ (odd) (the waiting time is $T_w^{(c)}$). In our estimates, in addition to $r_{\text{bs}} = 0.2$ and $\xi = 0.9$, we used the transmittance $\eta(L) = 10^{-\kappa L/10}$ with the attenuation coefficient $\kappa = 0.2$ dB/km describing losses in an optical fiber. It can be seen that the estimated waiting times that fall within the range of milliseconds may favorably compare with the lifetimes reported in Refs. [71–73].

V. TELEPORTATION

It is well known that shared entanglement is a resource of vital importance in fundamental quantum communication protocols such as quantum teleportation. The above discussed entanglement generation procedure provides this resource through the phase-modulated cat states entangled between the remote nodes. In this section we demonstrate how such entanglement can be utilized to teleport phase information from an SCW state resulting from the output state of the electro-optic modulator [see Eq. (4)]. In order to develop some intuition on how the teleportation procedure works, we consider the simplest case where Alice and Bob share a single-mode entangled coherent cat state,

$$|\Psi_v^{(AB)}(\alpha, \alpha)\rangle = \frac{1}{\sqrt{M_v(\alpha, \alpha)}} \{ |\alpha, \alpha\rangle_{AB} + v |-\alpha, -\alpha\rangle_{AB} \}, \quad (54)$$

where $M_\pm(\alpha, \alpha) = 2(1 \pm \exp[-4|\alpha|^2])$ is the normalization constant. Charlie at Alice's site possesses the SCW

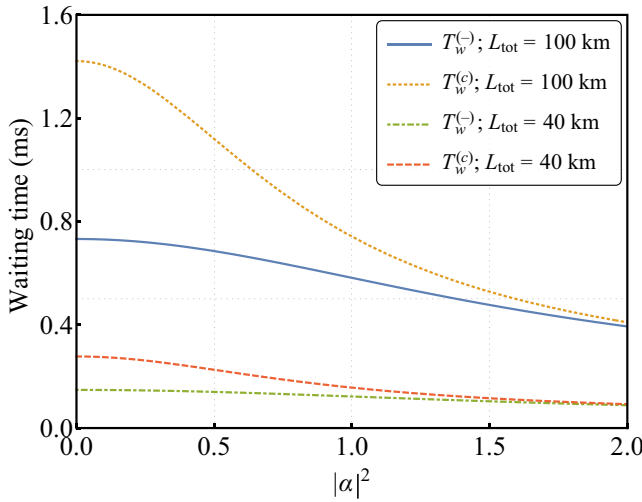


FIG. 7. Dependence of waiting times, $T_w^{(-)}$ and $T_w^{(c)}$, on $|\alpha|^2$ computed from Eq. (53) for swapping between identical links with $p_1 = p_2 = 2P_s^{(-)}$ (odd) and $p_1 = p_2 = 2P_s^{(c)}$ (odd), respectively. The quantum channel transmittance is taken to be $\eta(L) = 10^{-\kappa L/10}$ with $\kappa = 0.2$ dB/km, $L = 25$ km and the photon-number ratio r_{bs} is 0.2.

state [see Eq. (4)] with amplitude $|\alpha|$ and phase ϕ_c of the SCW state that is targeted for teleportation,

$$|\Psi_{scw}\rangle = |\gamma\rangle_C, \quad \gamma_\mu = U_{\mu 0}^{(C)*} \alpha \approx J_\mu(m_C) e^{i\mu\phi_c} \alpha, \quad (55)$$

where we assume that the phase coherence between Alice and Charlie is maintained. Thus, the joint state of the Alice, Bob, and Charlie tripartite system is

$$|S_{CAB}^{(v)}\rangle = |\Psi_{scw}\rangle \otimes |\Psi_v^{(AB)}(\alpha, \alpha)\rangle, \quad |\Psi_{scw}\rangle = |\gamma\rangle_C. \quad (56)$$

The scheme of the teleportation from Charlie to Bob is depicted in Fig. 8(a). Transfer of phase information from Charlie's SCW state to Bob's state can be implemented in the following steps.

(1) Alice uses the modulator with the modulation frequency and index identical to Charlie's to modulate her share of state (54) at phase ϕ_a .

(2) Charlie's and Alice's states are interfered on a 50 : 50 beam splitter.

(3) For the selected sideband, the presence of a single photon at the output channels of the beam splitter is monitored by two single-photon detectors, D_1 and D_2 .

(4) After a photon is registered by a photodetector, Alice communicates the result to Bob and he shifts the phase of his state depending on which detector is clicked. Charlie's SCW phase thus appears to be transferred to the phase of Bob's single-mode coherent state.

Below we describe these steps in detail. Phase modulation applied by Alice transforms the shared entangled state (56) as follows:

$$|S_{CAB}^{(v)}\rangle \mapsto |\Psi_{CAB}^{(v)}\rangle = |\gamma\rangle_C \otimes |\Psi_v^{(AB)}(\alpha, \beta)\rangle, \quad (57)$$

$$\alpha_\mu = U_{\mu 0}^{(A)*} \alpha \approx J_\mu(m_C) e^{i\mu\phi_a} \alpha.$$

Here the modulation indices of Charlie and Alice are assumed to be identical, so that $|U_{\mu 0}^{(A)}| = |U_{\mu 0}^{(C)}| \equiv |U_{\mu 0}|$ and $J_\mu(m_A) = J_\mu(m_C)$.

After Alice's and Charlie's modes are brought into interference onto the 50:50 beam splitter, the output state after the beam splitter

$$\begin{aligned} \hat{T}_{\gamma\alpha \rightarrow D_1 D_2} |\Psi_{CAB}^{(v)}\rangle &= |\Psi_{D_1 D_2 B}^{(v)}\rangle \\ &= \frac{1}{\sqrt{M_v(\alpha, \alpha)}} \left\{ |\gamma_+\rangle_{D_1} \otimes |\gamma_-\rangle_{D_2} \otimes |\alpha\rangle_B \right. \\ &\quad \left. + v |\gamma_-\rangle_{D_1} \otimes |\gamma_+\rangle_{D_2} \otimes |-\alpha\rangle_B \right\}, \end{aligned} \quad (58)$$

where $\gamma_\pm = \frac{1}{\sqrt{2}}(\gamma \pm \alpha)$, has the two modes $|\gamma_\pm\rangle_{D_1}$ and $|\gamma_\pm\rangle_{D_2}$ monitored by the detectors D_1 and D_2 , respectively.

For the sake of simplicity, in the limit of low amplitudes $|\alpha| \ll 1$, we truncate the Hilbert space up to a single photon. For an ideal single-photon detector that measures the sideband with index μ at the D_1 (D_2) channel, detection of a single photon will project state (58) onto the one-photon state $|\Phi_\mu^{(1)}\rangle = |1_\mu\rangle_{D_1} \otimes |0\rangle_{D_2}$ ($|\Phi_\mu^{(2)}\rangle = |0\rangle_{D_1} \otimes |1_\mu\rangle_{D_2}$), where $|1_\mu\rangle \equiv |0, \dots, 0, 1_\mu, 0, \dots, 0\rangle$ is the μ th sideband one-photon state, as follows:

$$|\Psi_{D_1 D_2 B}^{(v)}\rangle \mapsto |\Psi_B^{(v, \mu, i)}\rangle = \langle \Phi_\mu^{(i)} | \Psi_{D_1 D_2 B}^{(v)} \rangle / \sqrt{P_\mu^{(v)}}, \quad (59)$$

$$P_\mu^{(v)} = |\langle \Phi_\mu^{(i)} | \Psi_{D_1 D_2 B}^{(v)} \rangle|^2 = |U_{\mu 0}|^2 P^{(v)}, \quad (60)$$

$$P^{(v)} = \frac{|\alpha|^2}{1 + v e^{-4|\alpha|^2}} e^{-2|\alpha|^2}. \quad (61)$$

Here $P_\mu^{(v)}$ is the probability to detect a single photon in the μ th sideband by a photodetector. Since $\gamma_\mu \pm \alpha_\mu = |U_\mu| \alpha (\exp(i\mu\phi_c) \pm \exp(i\mu\phi_a))$, the post-measurement state of Bob (up to the global phase) can be written in the following explicit form:

$$|\Psi_B^{(v, \mu, 1)}\rangle \equiv |\Psi_B^{(v\phi)}\rangle = \cos(v\phi/2) |\alpha\rangle + i \sin(v\phi/2) |-\alpha\rangle, \quad \phi = \mu(\phi_c - \phi_a), \quad (62)$$

$$|\Psi_B^{(v, \mu, 2)}\rangle = |\Psi_B^{(v, \mu, 1)}\rangle \Big|_{\alpha \rightarrow -\alpha}. \quad (63)$$

When the clicked detector is changed from D_1 to D_2 , relation (63) shows that Bob needs to apply the π shift changing α to $-\alpha$ so as to have the same teleported state.

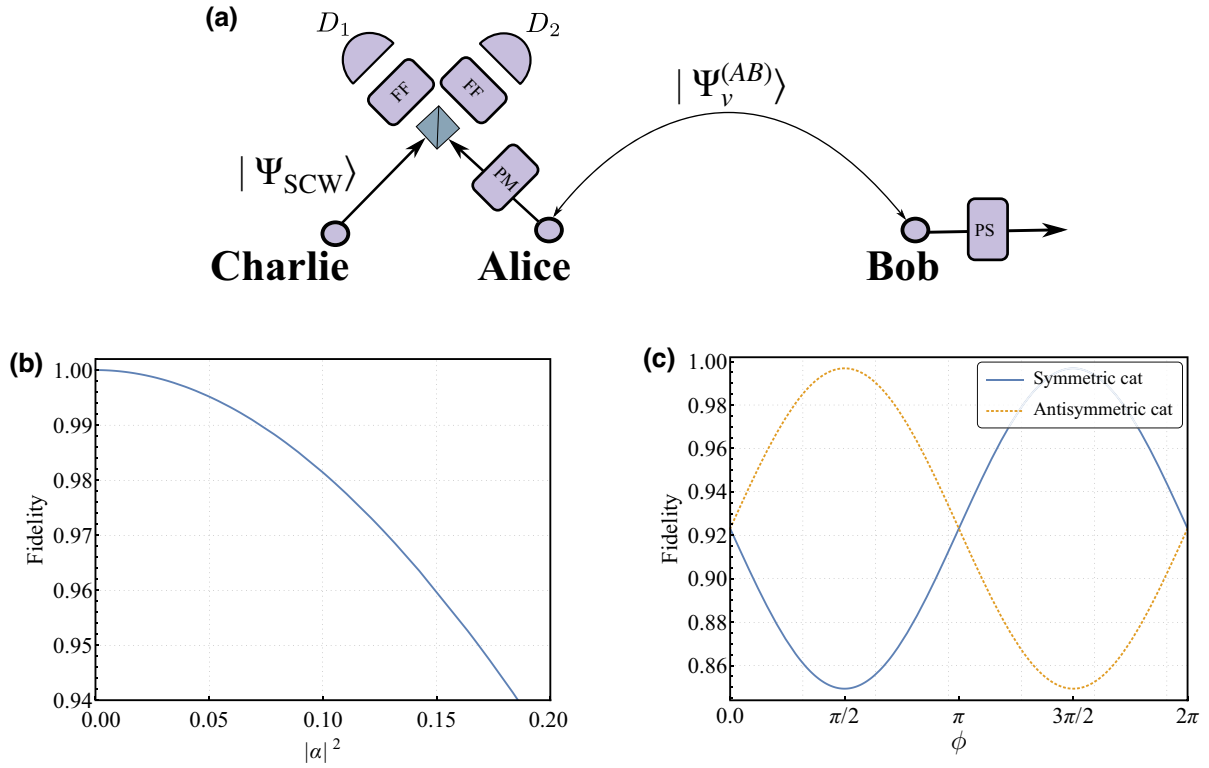


FIG. 8. (a) The teleportation scheme to transfer the SCW phase from Charlie to Bob using the entangled Schrödinger cat state. Here PM is the phase modulator, FF is the frequency filter, PS is the phase shifter, and D_1 and D_2 are the photodetectors. (b) Fidelity between $|\alpha\rangle$ and $\frac{1}{\sqrt{2}}(|\alpha\rangle - i|-\alpha\rangle)$ as a function of the amplitude $|\alpha|$ computed using Eq. (65). (c) Dependence of the fidelity given by Eq. (65) between $|\alpha e^{i\phi}\rangle$ and $\frac{1}{\sqrt{2}}(|\alpha\rangle_B \mp i|-\alpha\rangle_B)$ on the phase ϕ at $|\alpha| = 0.2$.

For the special case, where $\phi_c - \phi_a \in \{0, \pi/2, \pi, 3\pi/2\}$ and $\mu = \pm 1$, Table I summarizes how Charlie's SCW phase is mapped into the phase of Bob's coherent state provided Alice's phase vanishes ($\phi_a = 0$) and the cat state is symmetric ($\nu = 1$). Clearly, the teleported state exactly reproduces Charlie's phase when it is either 0 or π . In this table we used the approximation $\frac{1}{\sqrt{2}}(|\alpha\rangle_B \pm i|-\alpha\rangle_B) \approx |\mp i\alpha\rangle_B$ with the fidelity plotted in Figs. 8(b) and 8(c).

More generally, in the low-amplitude (mean photon-number) region where $|\alpha|$ is small, the teleported state can

be well approximated by the coherent state

$$|\Psi_B^{(\phi)}\rangle = \cos(\phi/2)|\alpha\rangle + i \sin(\phi/2)|-\alpha\rangle \approx |e^{-i\phi}\alpha\rangle. \quad (64)$$

The latter can be seen from the fidelity between $|\Psi_B^{(\phi)}\rangle$ and $|e^{-i\psi}\alpha\rangle$ given by

$$\begin{aligned} |\langle e^{-i\psi}\alpha | \Psi_B^{(\phi)} \rangle|^2 &= e^{-2|\alpha|^2} |\cos(\phi/2) \exp(e^{i\psi}|\alpha|^2) \\ &\quad + i \sin(\phi/2) \exp(-e^{i\psi}|\alpha|^2)|^2 \approx 1 \\ &\quad + 2(\cos(\phi - \psi) - 1)|\alpha|^2 + \dots, \end{aligned} \quad (65)$$

where the last equality is the fidelity expanded into a power series over $|\alpha|$ up to second order. Figure 8(b) illustrates that, at $\phi = -\pi/2$, the fidelity can be higher than 99% when the amplitude $|\alpha|$ is smaller than 0.25.

It is rather straightforward to generalize our analysis to the nonsymmetric case, where the amplitudes, $|\gamma|$, $|\alpha|$, and $|\beta|$, which determine Charlie's, Alice's, and Bob's states, respectively, differ from each other. In this case, Alice and

TABLE I. Truth table for the heralded state at Bob's site $|\Psi_B\rangle$ after performing teleportation with entangled coherent state $|\Psi_+^{(AB)}\rangle$ depending on the sideband registered, the photodetector that clicks, and the value of Charlie's SCW phase.

ϕ_c	D_1 clicks		D_2 clicks	
	+1 sideband	-1 sideband	+1 sideband	-1 sideband
ϕ_a	$ \alpha\rangle$	$ \alpha\rangle$	$ -\alpha\rangle$	$ -\alpha\rangle$
$\phi_a + \pi$	$ -\alpha\rangle$	$ -\alpha\rangle$	$ \alpha\rangle$	$ \alpha\rangle$
$\phi_a + \pi/2$	$ -\alpha\rangle$	$ i\alpha\rangle$	$ i\alpha\rangle$	$ -\alpha\rangle$
$\phi_a + 3\pi/2$	$ i\alpha\rangle$	$ -\alpha\rangle$	$ -\alpha\rangle$	$ i\alpha\rangle$

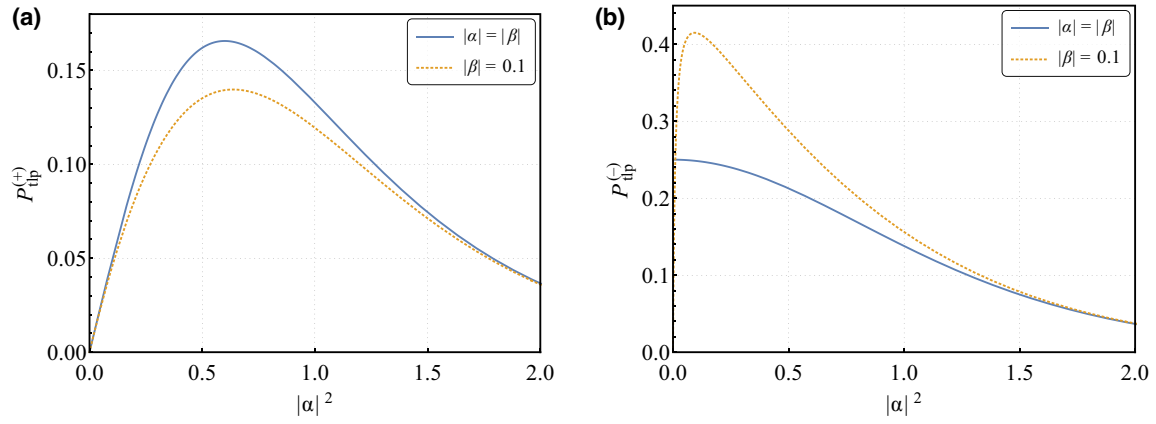


FIG. 9. Dependence of the success probabilities of teleportation, $P_{\text{tlp}}^{(\pm)}$, on the squared amplitude $|\alpha|^2$ computed from Eq. (70).

Bob share the state

$$\begin{aligned} |S_{AB}^{(v)}\rangle &= |\Psi_v^{(AB)}(\alpha, \beta)\rangle \\ &= \frac{1}{\sqrt{M_v(\alpha, \beta)}} \{ |\alpha\rangle_A \otimes |\beta\rangle_B + v |-\alpha\rangle_A \otimes |-\beta\rangle_B \}, \end{aligned} \quad (66)$$

where $M_v(\alpha, \beta) = 2(1 + v \exp[-2(|\alpha|^2 + |\beta|^2)])$, while Charlie holds state (55) with $\gamma_\mu = U_{\mu 0}^{(C)*} \gamma$.

Once Alice has applied the phase modulation to her mode and interfered it with Charlie's state on the 50:50 beam splitter, a single-photon detection in the sideband μ heralds preparation of the following state at Bob's node:

$$|\Psi_B^{(v, \mu, 1)}\rangle = \frac{(\gamma e^{i\phi_C} + \alpha e^{i\phi_A})|\beta\rangle + v(\gamma e^{i\phi_C} - \alpha e^{i\phi_A})|-\beta\rangle}{\sqrt{2(|\gamma|^2 + |\alpha|^2 + (|\gamma|^2 - |\alpha|^2)e^{-2|\beta|^2})}}, \quad (67)$$

$$|\Psi_B^{(v, \mu, 2)}\rangle = |\Psi_B^{(v, \mu, 1)}\rangle \Big|_{\beta \rightarrow -\beta}. \quad (68)$$

In which the probability of success is given by

$$\begin{aligned} P_{\mu, \text{tlp}}^{(v)} &= |U_{\mu 0}|^2 P_{\text{tlp}}^{(v)}, \\ P_{\text{tlp}}^{(v)} &= \frac{|\gamma|^2 + |\alpha|^2 + (|\gamma|^2 - |\alpha|^2)e^{-2|\beta|^2}}{2(1 + v e^{-2(|\alpha|^2 + |\beta|^2)})} e^{-|\alpha|^2 - |\gamma|^2}, \end{aligned} \quad (69)$$

Note that, since $P_{\text{tlp}}^{(-)} > P_{\text{tlp}}^{(+)}$, using the antisymmetric entangled coherent state $|\Psi_{-}^{(AB)}\rangle$ generally yields a higher teleportation rate as compared with the symmetric one $|\Psi_{+}^{(AB)}\rangle$, as can be seen from the curves shown in Fig. 9.

These curves represent $|\alpha|^2$ dependencies of $P_{\text{tlp}}^{(\pm)}$ computed at $|\alpha| = |\gamma|$ from

$$P_{\text{tlp}}^{(v)}(|\alpha|, |\beta|) = \frac{|\alpha|^2}{2(1 + v e^{-2(|\alpha|^2 + |\beta|^2)})} e^{-2|\alpha|^2}. \quad (70)$$

Figure 9 presents the results for two cases: the curves computed at $|\alpha| = |\beta|$ [$P_{\text{tlp}}^{(v)}(|\alpha|, |\alpha|)$ is given by Eq. (61)] and those where the amplitude of β is fixed [see Eq. (70)]. From Eq. (70) it is not difficult to see that $P_{\text{tlp}}^{(+)}(|\alpha|, |\alpha|) > P_{\text{tlp}}^{(+)}(|\alpha|, |\beta|)$ and $P_{\text{tlp}}^{(-)}(|\alpha|, |\alpha|) < P_{\text{tlp}}^{(-)}(|\alpha|, |\beta|)$ at $|\alpha| > |\beta|$. As shown in Fig. 9(a), for symmetric cats, all the curves are qualitatively similar and the maximum value of $P_{\text{tlp}}^{(+)}(|\alpha|, |\alpha|)$ reached at $|\alpha| = |\alpha|_{\text{max}}$ gives the highest probability provided $|\beta| < |\alpha|_{\text{max}}$.

For teleportation using antisymmetric cats, the behavior of teleportation success probabilities is strikingly different. Referring to Fig. 9(b), $P_{\text{tlp}}^{(-)}(|\alpha|, |\alpha|)$ starts from its maximal value 1/4 [$P_{\text{tlp}}^{(-)}(|\alpha|, |\alpha|)$ tends to 1/4 at $|\alpha| \rightarrow 0$] and monotonically decays to zero as $|\alpha|$ increases. By contrast, the curve for $P_{\text{tlp}}^{(-)}(|\alpha|, |\beta|)$ is similar to $P_{\text{tlp}}^{(+)}$. At sufficiently small $|\beta|$, the maximum of $P_{\text{tlp}}^{(-)}(|\alpha|, |\beta|)$ is above 1/4 and can be close to the limiting value 1/2. This is the case giving the highest success probability of teleportation.

Our concluding remark concerns the small mean photon-number approximation in Eq. (64) applicable to Bob's state at $|\beta| < 0.2$. Such an approximation may be of practical value as a teleported Bob state appears to be quasi-Gaussian with the corresponding benefits of a Gaussian state control. In particular, the phase of Bob's state can be measured with moderate resources and designing apparatus for the single-shot measurement of a phase for the Schrödinger cat and coherent state simultaneously is no longer required.

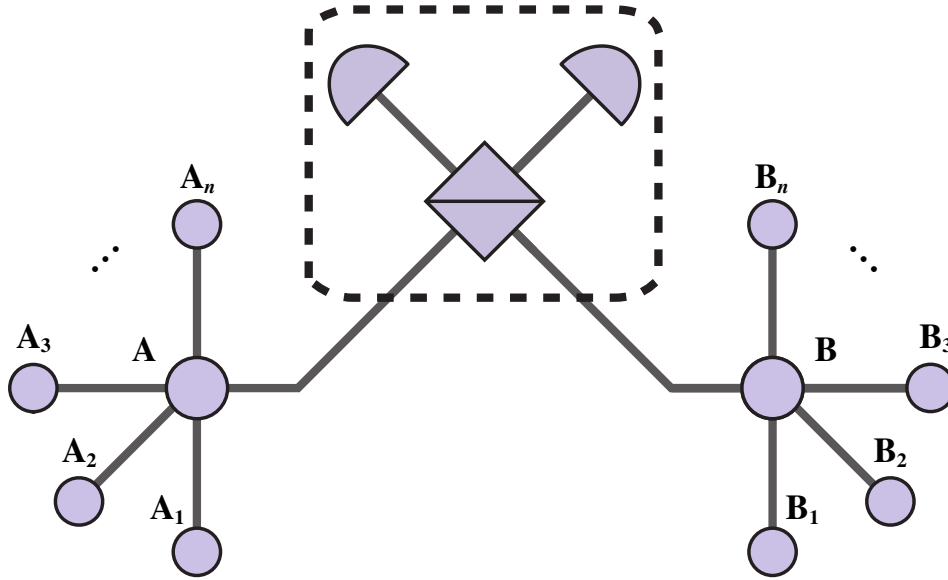


FIG. 10. Elementary link of an SCW quantum repeater in a star topology.

VI. CONCLUSIONS AND DISCUSSION

In this work we proposed use of phase-modulated multimode Schrödinger cat states for producing entanglement between remote parties (Alice and Bob) and for entanglement swapping. This approach to quantum repeaters is based on multimode coherent states generated by an electro-optic modulator and may reveal a number of interesting potential extensions.

For instance, as illustrated in Fig. 10, one of the advantages of using entangled multimode states is that the modes may, in principle, be distributed and stored in quantum memories located at different nodes of a star topology network. Since these modes differ in frequency, the dense wavelength division multiplexing demultiplexer can be employed to send them to different locations.

We analyzed the heralded entanglement generation scheme assuming that Alice and Bob send part of the modes that enter their multimode cat states, $|\Psi_{\nu'}^{(A)}\rangle$ and $|\Psi_{\nu}^{(B)}\rangle$, to the symmetric (50 : 50) beam splitter [see Fig. 1 and Eq. (16)] and computed the probabilities, $P_{\mu}^{(\nu'\nu)}$, for three orthogonal states (the vacuum state, $|\mathbf{0}\rangle$, the antisymmetric and modified symmetric cat states, $|\Phi_{-}\rangle$ and $|\Phi_{+}\rangle$) to occur at the output ports of the beam splitter for different couples (ν', ν) of input cats [see Eqs. (19) and (20)].

We modeled the optical fiber quantum channel with the transmittance η using the Stinespring dilation based on a beam splitter transformation for an enlarged system supplemented with environmental (noisy) modes [see Eq. (23)]. For the heralding events determined by the parity of photons, $p_c \in \{\text{odd}, \text{even}\}$, registered by a photodetector with efficiency ξ , we found that the conditional probabilities of detection (33) give the probabilities of success (36)

expressed in terms of $P_{\pm}^{(\nu'\nu)}$ with the renormalized mean photon-number ratio $r_{\text{bs}} \rightarrow \zeta = r_{\text{bs}}\eta\xi$.

It is shown that the fidelities, $F_{\mu}^{(\nu'\nu)}(p_c)$, between the density matrix of the heralded states (38) and the entangled cat states, $\Phi_{\mu}^{(AB)}$, can be described by two analytical expressions for the fidelities of predominantly symmetric and antisymmetric cats: $F_{-}^{(\pm)}$ (odd) and $F_{+}^{(\pm)}$ (even) given by Eqs. (41a) and (41b), respectively. It turned out that these fidelities characterizing the quality of the generated entanglement are monotonically decreasing functions of the amplitude $|\alpha|$ (see Fig. 5).

Our key analytical results are Eqs. (36) and (41) for the success probabilities and the fidelities describing performance and quality of the entanglement generation procedure. These results imply that producing high-quality entangled states requires the amplitude $|\alpha|$ to be sufficiently small. In this region, the highest values of the probability of success correspond to an odd number of clicks for either two antisymmetric input states (the heralded cat state is predominantly antisymmetric) or two states of different symmetry (the heralded cat state is predominantly symmetric). By contrast, in the low-amplitude region, the success probability for a couple of input symmetric cat states is negligibly small [see Eq. (37a)].

Note that, in reality, we have two detectors and each of the detectors registers the odd (even) number of photons with the same probability of success $P_s^{(\nu'\nu)}$ (odd) ($P_{\pm}^{(\nu'\nu)}$ (even)). The difference between the corresponding heralded states, $|\Psi_{\mu}^{(AB)}(\alpha_{\text{qm}}, \alpha_{\text{qm}})\rangle$ and $|\Psi_{\mu}^{(AB)}(\alpha_{\text{qm}}, -\alpha_{\text{qm}})\rangle$, can be corrected by applying a π shift to the phases of the modes at either Alice's or Bob's site. It means that the total performance of

entanglement generation can be characterized by twice the success probability.

For the generation of antisymmetric cats, this probability cannot be higher than 50% because $P_s^{(-)}(\text{odd}) \leq 1/4$ (see Fig. 4). Interestingly, $P_s^{(-)}(\text{odd})$ is identically equal to 1/4 when the product $\zeta \equiv r_{\text{bs}}\eta\xi$ is 1/2 [or, equivalently, $r_{\text{bs}} = r_{1/2} = 1/(2\eta\xi)$]. On the other hand, according to Fig. 5, the photon-number ratio r_{bs} should be lowered to enhance the quality of entanglement with the maximum value of fidelity $F_{-}^{(\pm)}(\text{odd})$ exceeding 90%.

By contrast, when the input cat states differ in symmetry and the heralded states are symmetric cats, double the probability of success $2P_s^{(e)}(\text{odd})$ is above 1/2 at $r_{\text{bs}} > r_{1/2}$ (see Fig. 4). In addition, as shown in Fig. 5, the maximum value of $F_{+}^{(e)}(\text{odd})$ reached at $|\alpha| = 0$ is unity. So, the procedure leading to entangled symmetric cats is superior to that for the case of antisymmetric ones in both performance and quality.

However, given the symmetric cat states efficiently produced to create entanglement between the nodes of elementary links, the success probability for entanglement swapping given by Eq. (47) will be close to zero. Therefore, antisymmetric cat states play an important part in reaching a reasonably high performance of the repeater. An important point is that there is a trade-off between the probability of success and fidelity (46) that needs to be optimized.

Part of our considerations assume that the modes can be stored in a multimode quantum memory [46,50]. For the repeater with two links, we estimated the so-called waiting time (53) giving the lower bound for the storage time of the quantum memory. The results presented in Fig. 7 show that the waiting time falls within the range of hundreds of microseconds for tens of kilometer long distances. For instance, according to Ref. [52], QMs based on atomic frequency comb protocol with rare-earth-ion doped crystals are promising multimode QMs that may tolerate such waiting times. The efficiency of such QMs, however, still needs to be improved.

Alternatively, our system may operate without a multimode QM. In this approach, the carrier mode at the central frequency is the only mode to be stored in the QM, whereas the sidebands are distributed over the repeater nodes. After extracting this mode from the memory, remodulation can be carried out and then the carrier mode can be stored again. High efficiency of the electro-optic modulator allows such a process to be recurring in cycles.

Thus, our analysis suggests feasibility of the proposed scheme for antisymmetric cat states and relatively short distances to the central node. In general, approaches to QRs using phase modulation to produce and control multimode states may lead to promising methods for the generation and distribution of entanglement. The quantum teleportation protocol that uses the entangled cat states to transfer the phase information

between remote parties discussed in Sec. V exemplifies one such method. Interestingly, one of our findings is that the antisymmetric cat states are superior to symmetric ones in teleportation performance.

ACKNOWLEDGMENTS

The work was done by the Leading Research Center “National Center for Quantum Internet” of ITMO University by order of JSCo Russian Railways. The work of ADK was also financially supported by the Ministry of Education and Science of the Russian Federation (Passport No. 2019-0903). E.S.M. and S.A.M. appreciate support within framework project no. 00075-02-2020-051/1 from 02.03.2020.

-
- [1] N. Gisin and R. Thew, Quantum communication, *Nat. Photonics* **1**, 165 (2007).
 - [2] M. Krenn, M. Malik, T. Scheidl, R. Ursin, and A. Zeilinger, in *Optics in Our Time* (Springer International Publishing, Cham, 2016).
 - [3] N. Gisin, G. Ribordy, W. Tittel, and H. Zbinden, Quantum cryptography, *Rev. Mod. Phys.* **74**, 145 (2002).
 - [4] F. Xu, X. Ma, Q. Zhang, H.-K. Lo, and J.-W. Pan, Secure quantum key distribution with realistic devices, *Rev. Mod. Phys.* **92**, 025002 (2020).
 - [5] V. Giovannetti, S. Lloyd, and L. Maccone, Advances in quantum metrology, *Nat. Photonics* **5**, 222 (2011).
 - [6] G. Tóth and I. Apellaniz, Quantum metrology from a quantum information science perspective, *J. Phys. A: Math. Theor.* **47**, 424006 (2014).
 - [7] E. T. Khabiboulline, J. Borregaard, K. De Greve, and M. D. Lukin, Optical interferometry with quantum networks, *Phys. Rev. Lett.* **123**, 070504 (2019).
 - [8] R. Van Meter and S. J. Devitt, The path to scalable distributed quantum computing, *Computer* **49**, 31 (2016).
 - [9] A. Yimsiriwattana and S. J. Lomonaco Jr., in *Quantum Information and Computation II*, edited by E. Donkor, A. R. Pirich, and H. E. Brandt (SPIE, Orlando, Florida, United States, 2004), p. 360.
 - [10] H.-J. Briegel, W. Dür, J. I. Cirac, and P. Zoller, Quantum repeaters: The role of imperfect local operations in quantum communication, *Phys. Rev. Lett.* **81**, 5932 (1998).
 - [11] N. Sangouard, C. Simon, H. de Riedmatten, and N. Gisin, Quantum repeaters based on atomic ensembles and linear optics, *Rev. Mod. Phys.* **83**, 33 (2011).
 - [12] W. J. Munro, K. Azuma, K. Tamaki, and K. Nemoto, Inside quantum repeaters, *IEEE J. Sel. Top. Quantum. Electron.* **21**, 78 (2015).
 - [13] S. Muralidharan, L. Li, J. Kim, N. Lütkenhaus, M. D. Lukin, and L. Jiang, Optimal architectures for long distance quantum communication, *Sci. Rep.* **6**, 20463 (2016).
 - [14] K. Azuma, S. E. Economou, D. Elkouss, P. Hilaire, L. Jiang, H.-K. Lo, and I. Tzitrin, Quantum repeaters: From quantum networks to the quantum internet, *ArXiv:2212.10820* (2022).

- [15] L.-M. Duan, M. D. Lukin, J. I. Cirac, and P. Zoller, Long-distance quantum communication with atomic ensembles and linear optics, *Nature* **414**, 413 (2001).
- [16] A. I. Lvovsky, B. C. Sanders, and W. Tittel, Optical quantum memory, *Nat. Photonics* **3**, 706 (2009).
- [17] K. Azuma, K. Tamaki, and H.-K. Lo, All-photon quantum repeaters, *Nat. Commun.* **6**, 6787 (2015).
- [18] M. Zwerger, A. Pirker, V. Dunjko, H. J. Briegel, and W. Dür, Long-range big quantum-data transmission, *Phys. Rev. Lett.* **120**, 030503 (2018).
- [19] Z. Su, J. Guan, and L. Li, Efficient quantum repeater with respect to both entanglement-concentration rate and complexity of local operations and classical communication, *Phys. Rev. A* **97**, 012325 (2018).
- [20] S. Wehner, D. Elkouss, and R. Hanson, Quantum internet: A vision for the road ahead, *Science* **362**, eaam9288 (2018).
- [21] K. Azuma, S. Bäuml, T. Coopmans, D. Elkouss, and B. Li, Tools for quantum network design, *AVS Quantum Sci.* **3**, 014101 (2021).
- [22] S.-H. Wei, B. Jing, X.-Y. Zhang, J.-Y. Liao, C.-Z. Yuan, B.-Y. Fan, C. Lyu, D.-L. Zhou, Y. Wang, G.-W. Deng, H.-Z. Song, D. Oblak, G.-C. Guo, and Q. Zhou, Towards real-world quantum networks: A review, *Laser Photonics Rev.* **16**, 2100219 (2022).
- [23] P. van Loock, N. Lütkenhaus, W. J. Munro, and K. Nemoto, Quantum repeaters using coherent-state communication, *Phys. Rev. A* **78**, 062319 (2008).
- [24] N. Sangouard, C. Simon, N. Gisin, J. Laurat, R. Tualle-Broui, and P. Grangier, Quantum repeaters with entangled coherent states, *J. Opt. Soc. Am. B* **27**, A137 (2010).
- [25] M. Ghasemi and M. K. Tavassoly, Toward a quantum repeater protocol based on the coherent state approach, *Laser Phys.* **29**, 085202 (2019).
- [26] B. C. Sanders, Entangled coherent states, *Phys. Rev. A* **45**, 6811 (1992).
- [27] B. C. Sanders, Review of entangled coherent states, *J. Phys. A: Math. Theor.* **45**, 244002 (2012).
- [28] W. J. Munro, G. J. Milburn, and B. C. Sanders, Entangled coherent-state qubits in an ion trap, *Phys. Rev. A* **62**, 052108 (2000).
- [29] H. Jeong, M. S. Kim, and J. Lee, Quantum-information processing for a coherent superposition state via a mixed entangled coherent channel, *Phys. Rev. A* **64**, 052308 (2001).
- [30] S. J. van Enk and O. Hirota, Entangled coherent states: Teleportation and decoherence, *Phys. Rev. A* **64**, 022313 (2001).
- [31] J.-L. Liu, R.-H. Shi, J.-J. Shi, G.-L. Lv, and Y. Guo, Quantum dual signature scheme based on coherent states with entanglement swapping, *Chin. Phys. B* **25**, 080306 (2016).
- [32] M. Sisodia, V. Verma, K. Thapliyal, and A. Pathak, Teleportation of a qubit using entangled non-orthogonal states: A comparative study, *Quantum Inf. Process.* **16**, 76 (2017).
- [33] S. R. Miry, Superposition of entangled coherent states: Physical realization and properties, *Theor. Math. Phys.* **100**, 1006 (2019).
- [34] Y.-S. Ra, A. Dufour, M. Walschaers, C. Jacquard, T. Michel, C. Fabre, and N. Treps, Non-Gaussian quantum states of a multimode light field, *Nat. Phys.* **16**, 144 (2020).
- [35] J.-M. MÉRolla, Y. Mazurenko, J.-P. Goedgebuer, and W. T. Rhodes, Single-photon interference in sidebands of phase-modulated light for quantum cryptography, *Phys. Rev. Lett.* **82**, 1656 (1999).
- [36] A. V. Gleim, V. I. Egorov, Y. V. Nazarov, S. V. Smirnov, V. V. Chistyakov, O. I. Bannik, A. A. Anisimov, S. M. Kynev, A. E. Ivanova, R. J. Collins, S. A. Kozlov, and G. S. Buller, Secure polarization-independent subcarrier quantum key distribution in optical fiber channel using BB84 protocol with a strong reference, *Opt. Express* **24**, 2619 (2016).
- [37] G. P. Miroshnichenko, A. V. Kozubov, A. A. Gaidash, A. V. Gleim, and D. B. Horoshko, Security of subcarrier wave quantum key distribution against the collective beam-splitting attack, *Opt. Express* **26**, 11292 (2018).
- [38] A. Gaidash, G. Miroshnichenko, and A. Kozubov, Subcarrier wave quantum key distribution with leaky and flawed devices, *J. Opt. Soc. Am. B* **39**, 577 (2022).
- [39] O. I. Bannik and E. S. Moiseev, Plug&play subcarrier wave quantum key distribution with deep modulation, *Opt. Express* **29**, 38858 (2021).
- [40] K. S. Mel'nik, N. M. Arslanov, O. I. Bannik, L. R. Gilyazov, V. I. Egorov, A. V. Gleim, and S. A. Moiseev, Using a heterodyne detection scheme in a subcarrier wave quantum communication system, *Bull. Russ. Acad. Sci.: Phys.* **82**, 1038 (2018).
- [41] E. Samsonov, R. Goncharov, A. Gaidash, A. Kozubov, V. Egorov, and A. Gleim, Subcarrier wave continuous variable quantum key distribution with discrete modulation: Mathematical model and finite-key analysis, *Sci. Rep.* **10**, 10034 (2020).
- [42] E. Samsonov, R. Goncharov, M. Fadeev, A. Zinoviev, D. Kirichenko, B. Nasedkin, A. Kiselev, and V. Egorov, Coherent detection schemes for subcarrier wave continuous variable quantum key distribution, *J. Opt. Soc. Am. B* **38**, 2215 (2021).
- [43] V. Chistiakov, A. Kozubov, A. Gaidash, A. Gleim, and G. Miroshnichenko, Feasibility of twin-field quantum key distribution based on multi-mode coherent phase-coded states, *Opt. Express* **27**, 36551 (2019).
- [44] E. Saglamyurek, N. Sinclair, J. Jin, J. A. Slater, D. Oblak, F. Bussi eres, M. George, R. Ricken, W. Sohler, and W. Tittel, Broadband waveguide quantum memory for entangled photons, *Nature* **469**, 512 (2011).
- [45] N. Sinclair, E. Saglamyurek, H. Mallahzadeh, J. A. Slater, M. George, R. Ricken, M. P. Hedges, D. Oblak, C. Simon, W. Sohler, and W. Tittel, Spectral multiplexing for scalable quantum photonics using an atomic frequency comb quantum memory and feed-forward control, *Phys. Rev. Lett.* **113**, 053603 (2014).
- [46] S. A. Moiseev and A. V. Gleim, *25th Annual International Laser Physics Workshop (LPHYS'16)*, Tech. Rep. (Yerevan Physics Institute, Yerevan, 2016).
- [47] K. T. Kaczmarek, P. M. Ledingham, B. Brecht, S. E. Thomas, G. S. Thekkadath, O. Lazo-Arjona, J. H. D. Munns, E. Poem, A. Feizpour, D. J. Saunders, J. Nunn, and I. A. Walmsley, High-speed noise-free optical quantum memory, *Phys. Rev. A* **97**, 042316 (2018).
- [48] R. Ikuta, T. Kobayashi, T. Kawakami, S. Miki, M. Yabuno, T. Yamashita, H. Terai, M. Koashi, T. Mukai, T. Yamamoto,

- and N. Imoto, Polarization insensitive frequency conversion for an atom-photon entanglement distribution via a telecom network, *Nat. Commun.* **9**, 1997 (2018).
- [49] J. H. Davidson, P. Lefebvre, J. Zhang, D. Oblak, and W. Tittel, Improved light-matter interaction for storage of quantum states of light in a thulium-doped crystal cavity, *Phys. Rev. A* **101**, 042333 (2020).
- [50] E. S. Moiseev, A. Tashchilina, S. A. Moiseev, and B. C. Sanders, Broadband quantum memory in a cavity via zero spectral dispersion, *New J. Phys.* **23**, 063071 (2021).
- [51] D. Lago-Rivera, S. Grandi, J. V. Rakonjac, A. Seri, and H. de Riedmatten, Telecom-heralded entanglement between multimode solid-state quantum memories, *Nature* **594**, 37 (2021).
- [52] M. F. Askarani, A. Das, J. H. Davidson, G. C. Amaral, N. Sinclair, J. A. Slater, S. Marzban, C. W. Thiel, R. L. Cone, D. Oblak, and W. Tittel, Long-lived solid-state optical memory for high-rate quantum repeaters, *Phys. Rev. Lett.* **127**, 220502 (2021).
- [53] P.-C. Wang, O. Pietx-Casas, M. F. Askarani, and G. C. do Amaral, Proposal and proof-of-principle demonstration of fast-switching broadband frequency shifting for a frequency-multiplexed quantum repeater, *J. Opt. Soc. Am. B* **38**, 1140 (2021).
- [54] P. J. Bustard, K. Bonsma-Fisher, C. Hnatovsky, D. Grobnic, S. J. Mihailov, D. England, and B. J. Sussman, Toward a quantum memory in a fiber cavity controlled by intracavity frequency translation, *Phys. Rev. Lett.* **128**, 120501 (2022).
- [55] M. Businger, L. Nicolas, T. S. Mejia, A. Ferrier, P. Goldner, and M. Afzelius, Non-classical correlations over 1250 modes between telecom photons and 979-nm photons stored in $^{171}\text{Yb}^{3+}:\text{Y}_2\text{SiO}_5$, *Nat. Commun.* **13**, 6438 (2022).
- [56] V. V. Dodonov, I. A. Malkin, and V. I. Man'ko, Even and odd coherent states and excitations of a singular oscillator, *Physica* **72**, 597 (1974).
- [57] J. S. Neergaard-Nielsen, B. M. Nielsen, C. Hettich, K. Mølmer, and E. S. Polzik, Generation of a superposition of odd photon number states for quantum information networks, *Phys. Rev. Lett.* **97**, 083604 (2006).
- [58] A. Ourjoumtsev, F. Ferreyrol, R. Tualle-Brouri, and P. Grangier, Preparation of non-local superpositions of quasi-classical light states, *Nat. Phys.* **5**, 189 (2009).
- [59] A. P. Lund, T. C. Ralph, and H. Jeong, Generation of distributed entangled coherent states over a lossy environment with inefficient detectors, *Phys. Rev. A* **88**, 052335 (2013).
- [60] T. Serikawa, J.-I. Yoshikawa, S. Takeda, H. Yonezawa, T. C. Ralph, E. H. Huntington, and A. Furusawa, Generation of a cat state in an optical sideband, *Phys. Rev. Lett.* **121**, 143602 (2018).
- [61] K. Takase, J.-I. Yoshikawa, W. Asavanant, M. Endo, and A. Furusawa, Generation of optical Schrödinger cat states by generalized photon subtraction, *Phys. Rev. A* **103**, 013710 (2021).
- [62] A. Ourjoumtsev, H. Jeong, R. Tualle-Brouri, and P. Grangier, Generation of optical “Schrödinger cats” from photon number states, *Nature* **448**, 784 (2007).
- [63] S. Puri, S. Boutin, and A. Blais, Engineering the quantum states of light in a Kerr-nonlinear resonator by two-photon driving, *npj Quantum Inf.* **3**, 18 (2017).
- [64] E. S. Moiseev, A. Tashchilina, S. A. Moiseev, and A. I. Lvovsky, Darkness of two-mode squeezed light in λ -type atomic system, *New J. Phys.* **22**, 013014 (2020).
- [65] A. Grimm, N. E. Frattini, S. Puri, S. O. Mundhada, S. Touzard, M. Mirrahimi, S. M. Girvin, S. Shankar, and M. H. Devoret, Stabilization and operation of a Kerr-cat qubit, *Nature* **584**, 205 (2020).
- [66] D. V. Sychev, A. E. Ulanov, A. A. Pushkina, I. A. Fedorov, M. W. Richards, P. Grangier, and A. I. Lvovsky, Generating and breeding optical Schrödinger’s cat states, *AIP Conf. Proc.* **1936**, 020018 (2018).
- [67] Z. Wang, Z. Bao, Y. Wu, Y. Li, W. Cai, W. Wang, Y. Ma, T. Cai, X. Han, J. Wang, Y. Song, L. Sun, H. Zhang, and L. Duan, A flying Schrödinger’s cat in multipartite entangled states, *Sci. Adv.* **8**, eabn1778 (2022).
- [68] G. P. Miroshnichenko, A. D. Kiselev, A. I. Trifanov, and A. V. Gleim, Algebraic approach to electro-optic modulation of light: Exactly solvable multimode quantum model, *J. Opt. Soc. Am. B* **34**, 1177 (2017).
- [69] P. L. Kelley and W. H. Kleiner, Theory of electromagnetic field measurement and photoelectron counting, *Phys. Rev.* **136**, A316 (1964).
- [70] W. Vogel and D.-G. Welsch, *Quantum Optics* (Wiley-VCH, Berlin, 2006), 3rd ed., p. 508.
- [71] Y. Wu, J. Liu, and C. Simon, Near-term performance of quantum repeaters with imperfect ensemble-based quantum memories, *Phys. Rev. A* **101**, 042301 (2020).
- [72] V. Semenenko, X. Hu, E. Figueroa, and V. Perebeinos, Entanglement generation in a quantum network with finite quantum memory lifetime, *AVS Quantum Sci.* **4**, 012002 (2022).
- [73] J.-M. Mol, L. Esguerra, M. Meister, D. E. Bruschi, A. W. Schell, J. Wolters, and L. Wörner, Quantum memories for fundamental science in space, *Quantum Sci. Technol.* **8**, 024006 (2023).